OPEN ACCESS Freely available online

PLOS | ONE

Protection of Cardiomyocytes from the Hypoxia-Mediated Injury by a Peptide Targeting the Activator of G-Protein Signaling 8

Motohiko Sato[1]*, Masahiro Hiraoka[2], Hiroko Suzuki[1], Miho Sakima[1], Abdullah Al Mamun[1], Yukiko Yamane[2], Takayuki Fujita[2], Utako Yokoyama[2], Satoshi Okumura[3], Yoshihiro Ishikawa[2]

1 Department of Physiology, Aichi Medical University, Nagakute, Aichi, Japan, **2** Cardiovascular Research Institute, Yokohama City University School of Medicine, Fukuura, Yokohama, Japan, **3** Department of Physiology, Tsurumi University School of Dental Medicine, Yokohama, Japan

Abstract

Signaling via heterotrimeric G-protein is involved in the development of human diseases including ischemia-reperfusion injury of the heart. We previously identified an ischemia-inducible G-protein activator, activator of G-protein signaling 8 (AGS8), which regulates Gβγ signaling and plays a key role in the hypoxia-induced apoptosis of cardiomyocytes. Here, we attempted to intervene in the AGS8-Gβγ signaling process and protect cardiomyocytes from hypoxia-induced apoptosis with a peptide that disrupted the AGS8-Gβγ interaction. Synthesized AGS8-peptides, with amino acid sequences based on those of the Gβγ-binding domain of AGS8, successfully inhibited the association of AGS8 with Gβγ. The AGS8-peptide effectively blocked hypoxia-induced apoptosis of cardiomyocytes, as determined by DNA end-labeling and an increase in cleaved caspase-3. AGS8-peptide also inhibited the change in localization/permeability of channel protein connexin 43, which was mediated by AGS8-Gβγ under hypoxia. Small compounds that inhibit a wide range of Gβγ signals caused deleterious effects in cardiomyocytes. In contrast, AGS8-peptide did not cause cell damage under normoxia, suggesting an advantage inherent in targeted disruption of the AGS8-Gβγ signaling pathway. These data indicate a pivotal role for the interaction of AGS8 with Gβγ in hypoxia-induced apoptosis of cardiomyocytes, and suggest that targeted disruption of the AGS8-Gβγ signal provides a novel approach for protecting the myocardium against ischemic injury.

Citation: Sato M, Hiraoka M, Suzuki H, Sakima M, Mamun AA, et al. (2014) Protection of Cardiomyocytes from the Hypoxia-Mediated Injury by a Peptide Targeting the Activator of G-Protein Signaling 8. PLoS ONE 9(3): e91980. doi:10.1371/journal.pone.0091980

Editor: Xin-Liang Ma, Thomas Jefferson University, United States of America

Received December 10, 2013; **Accepted** February 16, 2014; **Published** March 14, 2014

Funding: This work is supported by Grant-in-Aid for Scientific Research on Innovative Areas of Japan (MS), Grant-in-Aid for Scientific Research of Japan (MS), the Toyoaki Scholarship Foundation (MS), The Naito Foundation (MS) and Strategic Research Foundation Grant-aided Project for Private Universities from the Ministry of Education, Culture, Sports, Science, and Technology, Japan (MEXT), 2011–2015 (S1101027). The funders had no role in study design, data collection and analysis, decision to publish, or preparation of the manuscript.

Competing Interests: The authors have declared that no competing interests exist.

* E-mail: motosato@aichi-med-u.ac.jp

Introduction

Signaling mediated by heterotrimeric G-protein plays important roles in signal integration in cells. Heterotrimeric G-proteins are activated by G-protein–coupled receptors (GPCRs) at the cell surface in response to extra stimuli. The activation of G-protein signaling is associated with nucleotide exchange on the Gα subunits leading to a conformational change in Gαβγ and subsequent transduction of signals to various effector molecules [1]. However, a novel class of regulatory proteins that directly activate heterotrimeric G protein without receptor activation has been identified [2–4]. Such molecules are expected to provide alternative signaling via heterotrimeric G-protein and regulate signal adaptation during pathophysiologic stress [5].

The importance of accessory proteins for heterotrimeric G-protein has been reported in human diseases and animal models [5]. For example, activator of G-protein signaling 1 (AGS1) is a direct activator of the Gα subunit and involved in the secretion of atrial natriuretic factor in heart failure [6,7]. Further, regulators of G-protein signaling (RGSs), the group of proteins that inhibit G-protein signaling by accelerating the GTPase activity of the Gα subunit, are involved in various cardiovascular diseases, such as hypertension, cardiac hypertrophy, and hypoxia-mediated injury [8–10].

We have been focusing on identification of accessory proteins of heterotrimeric G-proteins induced in cardiovascular diseases and have found novel activators of G-protein signaling from the hypertrophied heart and during repetitive transient ischemia [11,12]. Thus, we identified TFE3 (AGS11), an AGS protein that selectively forms a complex with the Gα16 subunit and is upregulated in the hypertrophied hearts of mice [11]. TFE3 translocates Gα16 to the nucleus, which leads to the induction of claudin-14, a component of the membrane in cardiomyocytes. This suggests that the novel form of transcriptional regulation counteracts pressure overload.

Activator of G-protein signaling 8 (AGS8) is a Gβγ signal regulator isolated from a cDNA library of rat hearts subjected to repetitive transient ischemia [12]. In response to hypoxia, AGS8 is up-regulated in the myocardium and cultured adult cardiomyocytes. AGS8 interacts directly with Gβγ and promotes Gβγ signaling in cells [12]. Suppression of AGS8 inhibits hypoxia-induced apoptosis of cardiomyocytes, suggesting AGS8 is required for hypoxia-mediated cell death [13]. AGS8 complexes with

connexin 43 (CX43) to form a transmembrane channel for multiple small molecules, including calcium, adenosine, ATP, and reactive oxygen species [14–16]. AGS8 regulates phosphorylation of CX43 in a Gβγ-dependent manner and influences hypoxia-mediated internalization of cell-surface CX43 [13]. Therefore, the AGS8-Gβγ complex plays a critical role under hypoxic conditions, making the cellular environment more sensitive to hypoxic stress by influencing the permeability of molecules passing through CX43.

Ischemic injury of the heart is associated with activation of multiple signal cascades initiating intracellular ionic and chemical changes that lead to the death of cardiomyocytes [17,18]. A previous study indicated that AGS8-Gβγ is involved in the programs leading to cell death, and the formation of the AGS8-Gβγ complex appears to be a critical step triggering the apoptotic process [13]. If a tool to manipulate the AGS8-Gβγ interaction in cells were available, it might be a promising approach for protection of cardiomyocytes against hypoxia-mediated injury.

Here, we report the identification of the Gβγ-interface of AGS8 and a peptide (AGS8-peptide) designed to correspond to the domain of interaction between Gβγ and AGS8 that protects cardiomyocytes against hypoxia-induced apoptosis. The observations indicate the importance of the AGS8-Gβγ complex in hypoxia-mediated apoptosis of cardiomyocytes as well as the potential value of targeted disruption of the AGS8-Gβγ signal for protecting the myocardium against ischemic injury.

Experimental Procedures

Materials

Anti Gβ antibody was obtained from Santa Cruz Biotechnology. Anti CX43 antibody and IGEPAL CA-630 was obtained from Sigma. Gallein was purchased from Calbiochem. Cleaved caspase-3 andtibody was obtained from Cell Signaling Technology. Recombinant $G\beta_1\gamma_2$ was obtained from Calbiochem-Merck Millipore. MTT (3-(4,5-methylthiazol-2-yl)-2,5-diphenyltetrazolium bromide) was purchased from Dojindo Molecular Laboratories (Kumamoto, Japan).

Synthesis of Peptide

The peptides were synthesized and purified by Invitrogen and peptide identity was verified by matrix-assisted laser desorption ionization mass spectrometry. The peptides were dissolved in aliquots (10 mM) and immediately frozen at −70°C.

Generation of GST-fusion Protein, Protein Interaction Assays, and Immunoblotting

The segments of AGS8 (DQ256268) were amplified by PCR and fused in frame to GST in the pGEX-6T vector (Amersham Biotech). Each GST-partial-AGS8 fusion proteins were expressed in bacteria (*Escherichia coli* BL21, Amersham Biotech) and purified on a glutathione affinity matrix. The GST fusion protein was eluted from the resin, and glutathione was removed by desalting to allow a solution-phase interaction assay [19]. Protein interaction assays and immunoblotting were performed as described previously [19,20].

Preparation of Cardiomyocytes and Delivery of Peptide to Cells

Cardiomyocytes were prepared from the hearts of 1-3-day-old Wistar rats as described previously [13]. The neonates were deeply anesthetized with pentobarbital sodium (100 mg/kg) and decapitated for cardiac tissue harvesting. The ventricular cardiomyocytes were then enzymentically dissociated and seeded at 1.0×10^5 cell in 24 mm or 4.0×10^5 cell in 35 mm plates. Prepared cardiomyocytes were cultured in DMEM/F12 including Insulin–Transferrin–Selenite (ITS), 100 units/ml penicillin, 100 mg/ml streptomycin, and 10 mM glutamine, in 5% CO_2 at 37°C. In some experiments, cardiomyocytes were incubated in a hypoxic incubator (MODEL9200, Wakenyaku, Kyoto, Japan) equilibrated to 1% O_2, 5% CO_2, and 94% N_2 at 37°C. The cells were subjected to two different hypoxic challenges. In the first protocol, cardiomyocytes were exposed 3 times to 30 min of hypoxia with intermittent 30-min periods of normoxia to capture the early events caused by hypoxia in the living cells before they died. Particularly, internalization of cell-surface connexin 43 and changes in the permeability of connexin were analyzed. In the second protocol, cardiomyocytes were exposed to 1% O_2 for 6 h followed by 12 h of normoxia to induce hypoxia-mediated apoptosis. At the end of the second protocol, apoptotic cell death was analyzed. In some experiments, approximately 24 h after preparation, peptides were delivered to cardiomyocytes by using PLUSin (Polyplus, NY, USA) according to the manufacturer's instructions. Briefly, ~1.0 μg peptide was incubated with 2.0 μl of PLUSin in 100 μl supplied buffer for 15 min and then added the mixture to each dishes. This preparation typically provided 0.5 to 1 μM of peptide in the culture medium. The amount of peptide and the incubation time for peptide-delivery were optimized by analyzing incorporation of fluorescein isothiocyanate (FITC)-conjugated peptide into cardiomyocytes. In the condition used in this study, the chemical reagent for peptide delivery did not influence the number of living cells analyzed by trypan blue stain within 4 h treatment (0.75 μM peptide; 102.0±6.7%, 1.5 μM peptide; 90.5±5.0% versus no treatment control, not statistically significant, n = 4) [21].

Immunocytochemistry

Immunostaing of cultured cardiomyocytes was performed as described previously [13]. Briefly, cells were seeded on 24×24 mm polylysine-coated coverslips. Cells were fixed with 4% paraformaldehyde for 15 min and then incubated with 0.2% Triton X-100 for 5 min. After 1 h incubation of 5% normal donkey serum, cells were incubated with primary antibodies for 18 h at 4°C. Following 1 h incubation of secondary antibody (goat anti-mouse AlexaFluor 488 or goat anti-rabbit AlexaFluor 594, highly cross-absorbed, Molecular Probes), cells were incubated with 1 μg/ml 4′,6′-diamidino-2-phenylindole, dihydrochloride (DAPI) (Molecular Probes) in PBS for 5 min. Slides were then mounted with glass coverslips with ProLong Gold antifade reagent (Invitrogen). Images were analyzed by deconvolution microscopy (TE2000-E, Nikon, Tokyo, Japan). Obtained images were deconvoluted using NIS-Elements 3.0 software (Nikon) with a "no neighbors" deconvolution algorithm. All images were obtained from approximately the middle plane of the cells.

Dye Uptake Study

Up take of CX43 permeable fluorescence dye Lucifer Yellow (LY) (Molecular Probes) was performed as described previously [13]. Briefly, cardiomyocytes were incubated with 1 mM Lucifer Yellow (LY) (Molecular Probes) for 30 min. The fluorescence of LY was determined by fluorescence microscopy (B-3A filter, TE2000-E, NIKON, Tokyo, Japan) following removal of incorporated LY and rinse with PBS. The signal intensity was quantified in 10 randomly selected fields (10×20) using NIS-Elements 3.0 software (NIKON, Tokyo, Japan). The non-specific binding of LY was determined in the presence of a connexin hemichannel blocker, 50 mM of Lanthanum (Sigma-Aldrich).

In situ Assay for Apoptosis Detection

In situ labeling of fragmented DNA in cardiac myocytes was detected by TACS2 TdT-Blue Label In Situ Apoptosis Detection Kit (Travigen, Inc., Gaitherburg, MD), that detects DNA breaks in genomic DNA by enzymatic incorporation of biotinylated nucleotides followed by the binding of streptavidin-peroxidase conjugates, according to the manufacture's instructions. Briefly, myocytes were fixed with 3.7% formaldehyde in phosphate buffered saline (PBS) for 10 min and with 70% ethanol for 5 min and then incubated in proteinase K (0.02 mg/ml) at room temperature for 5 min. The cells were incubated with 2% hydrogen peroxide for 5 min and washed with labeling buffer consisting of 50 mM Tris (pH 7.5), 5 mM $MgCl_2$, 60 mM 2-mercaptoethanesulfonic acid, and 0.05% BSA, followed by 60 min of incubation at 37°C in labeling buffer containing 150 mM dATP, 150 mM dGTP, 150 mM dTTP, 5 mM biotinylated dCTP, and 40 U/ml of the Klenow fragment of DNA polymerase I. Untreated myocytes incubated with or without 2 mg/ml DNAse in the labeling buffer were used as positive or negative controls, respectively. The incorporated biotinylated dCTP was then detected with strepavidin-peroxidase conjugate and revealed in 0.5 mg/ml diaminobenzidine for 10 min. Nuclear brown staining was viewed under a light microscope.

MTT Assay

Cardiomyocytes in 24-well culture plates were incubated in PBS (pH 7.4) containing 0.5 mg/ml MTT at 37°C. After for 2 h incubation, the PBS was removed and 100 µl of dimethyl sulfoxide (DMSO) was added to each well to solubilize dark blue formazan products. Absorbance of the colored solution was determined at 595 nm [22].

Miscellaneous Procedures and Statistical Analysis

Immunoblotting and data analysis were performed as described previously [12,13]. The luminescence images captured with an image analyzer (LAS-3000, Fujifilm, Tokyo, Japan) were quantified using Image Gauge 3.4 (Fujifilm). Data are expressed as mean ± S.E.M. from independent experiments as described in the figure legends. Statistical analyses were performed using the unpaired *t* test, F-test, one-way ANOVA followed by Tukey's multiple comparison post-hoc test. All statistical analyses were performed with Prism 4 (GraphPad Software, USA).

Ethics Statement

Animal study was approved by the Institutional Animal Care and Use Committees of Yokohama City University.

Results

The C-terminal Region of AGS8 was Required to Activate Gβγ Signaling in Cells

To determine the region of interaction between Gβγ and AGS8, we divided the rat AGS8 (DQ256268) sequence into 6 segments and synthesized the segments as glutathione *S*-transferase (GST)-fusion proteins (Fig. 1*A*). Each of GST-AGS8 peptides was subjected to a pull-down assay to examine its interaction with purified Gβγ (Fig. 1*B*). The C-terminus of AGS8 (AGS8-C) successfully pulled down Gβγ, as documented in the previous manuscript [12]. Another segment, AGS8-254, also pulled down Gβγ to a lesser extent than AGS8-C, suggesting that a potential second Gβγ-interacting domain existed in this region. However, the remaining segments failed to pull down Gβγ.

Next, the bioactivity of each of the AGS8 regions was investigated by evaluating the activation the G-protein signaling pathway in Saccharomyces *cerevisiae* [12,23]. This yeast strain lacked the pheromone receptor, but expressed mammalian Gαs in place of the yeast Gα subunit and provided a read-out of growth upon activation of the G-protein–regulated pheromone signaling pathway [23]. The peptide corresponding to each AGS8 domain was subcloned in a galactose-inducible vector and introduced into the yeast strain [24]. The bioactivity in the G-protein pathway was examined be evaluating the galactose-dependent growth of the transformed yeast. Although each segment of AGS8 was expressed in the yeast cells, AGS8-C was the only segment able to activate G-protein signaling (Fig. 1*C*). Thus, we focused on AGS-C and explored the Gβγ-interaction site in this domain.

The FN3 Domain was Important for the Interaction of AGS8 with Gβγ

The sequence of AGS8-C (A^{1359} to W^{1730} of rat ABB82299) was further divided into smaller fragments that were synthesized as GST-fusion proteins in bacteria. Two fusion proteins of GST-AGS8-C, namely, AGS8-C1 (A^{1359}– H^{1493}) and AGS8-C2 (A^{1494} – T^{1585}), were successfully synthesized and migrated as expected on SDS-PAGE. While AGS8-C1 did not pull down purified Gβγ, AGS8-C2, which represented the FN3 domain, did pull down Gβγ, indicating the importance of the FN3 domain for the interaction of AGS8 with Gβγ (Fig. 1*D*).

AGS8-peptides Blocked the Interaction of AGS8C with Gβγ

To further determine the region of interaction between AGS8 and Gβγ, we prepared multiple 29- to 30-amino–acid peptides, the sequences of which were based on the amino acids from A^{1494} to W^{1730} of the rat AGS8 (ABB82299) (Fig. 2*A*). In a screen of 11 peptides by the GST-pull–down assay, which covered the entire region from A^{1494} to W^{1730} of the rat AGS8, we found two peptides, CP1 (A^{1494}PRNITVVAMEGCHSFVIVDWN-KAIPGDV^{1522}) and CP9 (S^{1508}FVIVDWNKAIPGDVVTGYL-VYSASYEDFI^{1537}) that effectively blocked the interaction of AGS8 with Gβγ in a dose-dependent manner (Fig. 2*B*). Quantitative analysis of immunoblots confirmed the dependence of the interaction of AGS8 with Gβγ on dose (Fig. 2*C*) and indicated that both peptides had similar IC50s (CP1:6.73×10^{-6} M; CP9:2.77×10^{-6} M). We first focused on CP9 and used this peptide as the AGS8-peptide in the following experiments.

The Gβγ-interaction Site of AGS8 was Localized at the FN3 Domain of the C-terminus of AGS8

The present data suggested that the first 45 amino acids of the FN3 domain represented by CP1 and CP2 were critical for AGS8 to interact with Gβγ and mediate signal to downstream molecules. The importance of this region for AGS8-mediated signaling was further examined in the yeast cells in which growth was linked to G-protein activation [23]. A deletion mutant of AGS8-C, which lacked the first 45 amino acids of this domain, failed to activate G-protein signaling, indicating the importance of this region for mediating AGS8-Gβγ signaling in the cell (Fig. 3).

The AGS8-peptide Inhibited Hypoxia-induced Internalization of Connexin 43 in Cardiomyocytes

In a previous study, we demonstrated that AGS8 was required for hypoxia-induced apoptosis of cardiomyocytes, which was associated with changes in the permeability of CX43 [13]. AGS8-Gβγ accelerates the internalization and degradation of channel

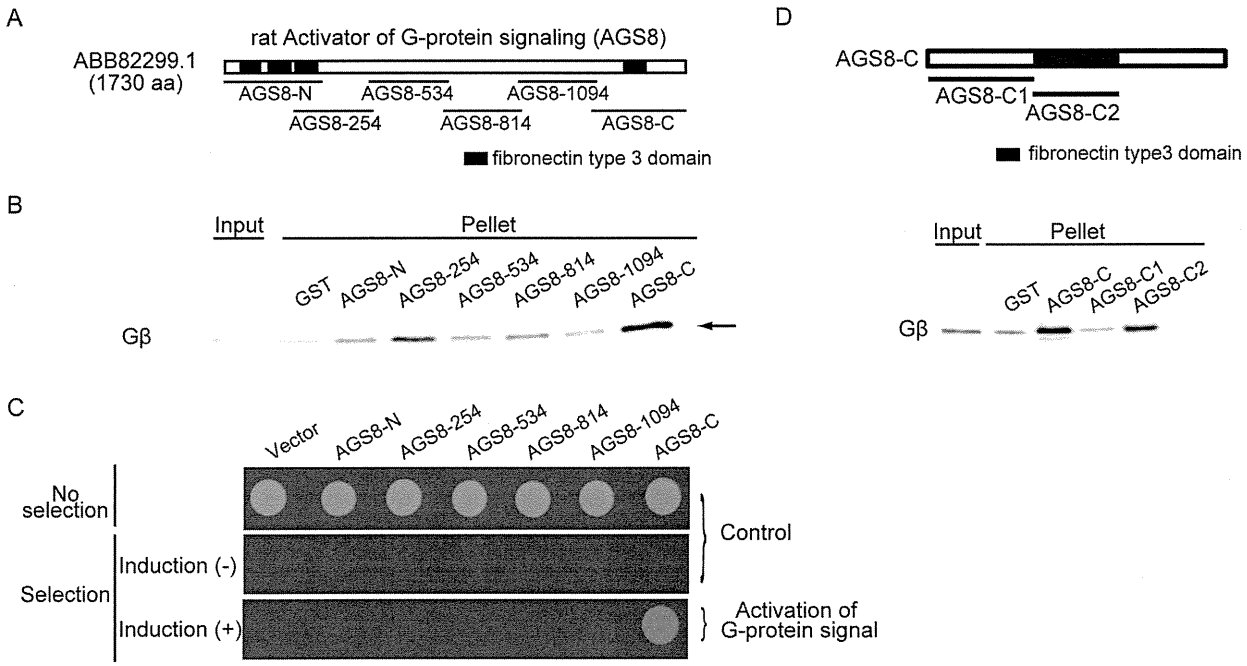

Figure 1. Determination of Gβγ interacting domain of the AGS8. (A) Schematic diagram of rat AGS8 and the AGS8 domains synthesized as GST-fusion proteins. Each GST protein fused with the following segment of rat AGS8 (ABB82299) respectively. AGS8-N: M^{1}- P^{370}, AGS8-254: A^{254}– R^{553}, AGS8-534: S^{534}– S^{833}, AGS8-814: S^{814}– R^{1113}, AGS8-1094: H^{1094}– D^{3280}, AGS8-C: A^{1359}– W^{1730}. (B) GST-pulldown assay of AGS8 domains with $G\beta_1\gamma_2$. AGS8 domains synthesized as GST-fusion proteins (300 nM) were incubated with recombinant human $G\beta_1\gamma_2$ (30 nM) in a total volume of 300 μl at 4°C. Proteins were then adsorbed to a glutathione matrix and retained G-protein subunits identified by immunoblotting following gel electrophoresis. The representative of 5 independent experiments with similar results. (C) Bioactivity of AGS8 domains on G-protein activation in cell. The yeast strain expressing human Gαs was transformed with AGS8 domains described in (A) into the pYES2-containing GAL1 promoter. The yeast strain was modified to grow without histidine on activation of G-protein. Induction(+): induction of translation of AGS8 domains by galactose. The representative of 4 independent experiments with similar results. (D) GST-pull down assay of AGS8-C segments with recombinant Gβγ. (*upper panel*) Schematic diagram of AGS8-C and the segments synthesized as GST-fusion proteins. Each GST protein fused with the following segment of rat AGS8 (ABB82299) respectively. AGS8-C1: A^{1359}– H^{1493}, AGS8-C2: A^{1494}– T^{1585}. (*lower panel*) GST-pulldown assay of AGS8 segments with $G\beta_1\gamma_2$. AGS8 domains synthesized as GST-fusion proteins (300 nM) were incubated with recombinant human $G\beta_1\gamma_2$ (30 nM) in a total volume of 300 μl at 4°C. Proteins were then adsorbed to a glutathione matrix and retained G-protein subunits identified by immunoblotting following gel electrophoresis. The representative of 4 independent experiments with similar results.
doi:10.1371/journal.pone.0091980.g001

protein CX43 under hypoxia, which results in decreased membrane permeability in the cardiomyocytes [13]. The change in localization and permeability of CX43 in the membrane is associated with hypoxia-induced apoptosis of the cardiomyocytes [14–16]. Therefore, we transferred the AGS8-peptide to cardiomyocytes and examined its effect on the internalization of CX43 induced by repetitive hypoxia (Fig. 4*A*).

The peptide was delivered to the cardiomyocytes by chemical reagent as described in "experimental procedures". Treatment of the cells with the chemical reagent and FITC-conjugated AGS8-peptide showed that the peptide was successfully delivered into the cardiomyocytes (Fig. 4*B*). The effect of the AGS8-peptide on internalization of CX43 was determined in the cardiomyocytes after hypoxic stress. CX43 was observed on the surface of the cardiomyocytes under normoxia (Fig. 4*B*), and its presence was decreased after exposure of the cardiomyocytes to repetitive hypoxia in the untransfected control cells and the cells exposed to transfection reagent alone (Fig. 4*B, 4C*). However, the AGS8-peptide dramatically blocked the internalization and degradation of CX43 induced by repetitive hypoxia (Fig. 4*B, 4C*). When the effect of FITC-conjugated AGS8-peptide was examined, FITC was observed in the cardiomyocytes under normoxia as well as hypoxia, and the hypoxia-induced internalization of CX43 was inhibited in FITC-positive cells (Fig. 4*B*).

The AGS8-peptide Inhibited the Decrease in Permeability of Connexin 43 Under Hypoxia

Loss of CX43 from the cell surface decreases influx and efflux of small molecules passing through CX43, and this effect is associated with apoptosis of the cardiomyocytes under hypoxia [13–16]. We next examined the ability of AGS8-peptide to block the change in permeability of CX43 by analyzing by the flux of the fluorescent dye, Lucifer Yellow (LY), which passes through CX43 as previously demonstrated [13]. LY in the culture medium was incorporated into cardiomyocytes under normoxia. The flux of dye was decreased after exposure of the cells to repetitive hypoxia in the control group as well as in the group exposed to transfection reagent alone (31.1±4.4%, 26.9±13.0%, respectively) (Fig. 5). However, the AGS8-peptide blocked the hypoxia-induced decrease in permeability in a dose-dependent manner. This observation is consistent with the immunofluorescence studies, in which CX43 was observed to remain at the cell surface after repetitive hypoxia in the presence of AGS8-peptide (Fig. 4).

The AGS8-peptide Protected Cardiomyocytes from Hypoxia-induced Apoptosis

To examine the effect of AGS8 peptide on apoptosis of the cardiomyocytes, cultured cardiomyocytes were sequentially ex-

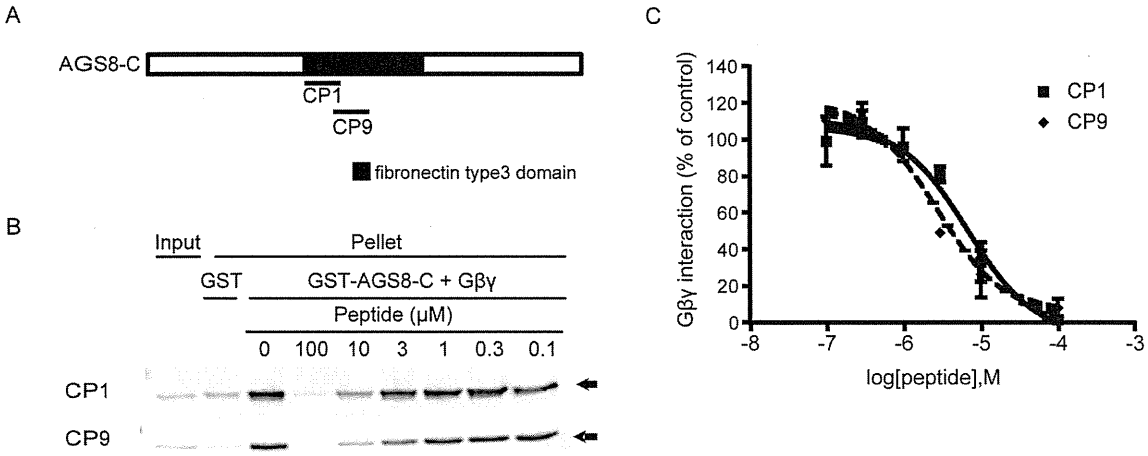

Figure 2. Development of AGS8 peptide. (A) Schematic diagram of AGS8-C and the AGS8-peptides (CP1 and CP9) which inhibited AGS8-Gβγ interaction. The AGS8-peptides were developed based on amino acid sequences of the Gβγ interaction domain of AGS8. CP1 and CP2 represented A^{1494}– V^{1522} and S^{1508}– I^{1537} of rat AGS8 (ABB82299) respectively. (B) The example of GST-pulldown assay of GST-AGS8-C with $G\beta_1\gamma_2$. GST-fusion protein (100 nM) was incubated with recombinant human $G\beta_1\gamma_2$ (10 nM) in the presence of AGS8-peptides (CP1 or CP9). Proteins were then adsorbed to a glutathione matrix and retained G-protein subunits identified by immunoblotting following gel electrophoresis. The representative of 6 independent experiments with similar results. (C) The densitometric analysis of GST-pulldown assay of GST-AGS8-C with $G\beta_1\gamma_2$ in the presence of AGS8-peptides. n = 6 with peptides of ~97% HPLC purity.
doi:10.1371/journal.pone.0091980.g002

posed to 1% oxygen for 6 h, then to 12 h of normoxia to induce hypoxia-mediated cell death (Fig. 6*A*) [13]. Hypoxia/reoxygenation markedly increased the number of apoptotic cardiomyocytes, as determined by TUNEL or immunostaining of cleaved caspase-3, in the untransfected control cells and those exposed to transfection reagent alone (Fig. 6B and 6C). However, AGS8-peptide successfully inhibited hypoxia-induced apoptosis, indicating a protective effect in cardiomyocytes. Additionally, the data indicated that, under normoxia, the AGS8-peptide did not influence apoptosis or the permeability of CX43 (Fig. 6*B and 6C*).

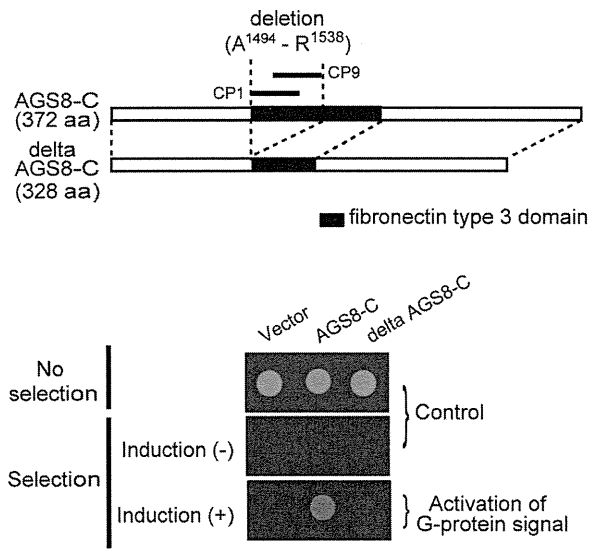

Figure 3. Effect of deletion of 45 amino acids of fibronectin type 3 domain. (A) Schematic diagram of C-terminal of AGS8 (AGS8-C) and the deleted mutant of AGS8-C (delta AGS8-C) lacking the first 45 amino acids of fibronectin type 3 domain, that are A^{1494} to R^{1538} of rat AGS8 (ABB82299). (B) Bioactivity of AGS8C and delta AGS8C on G-protein activation. The yeast strain expressing human Gαs was transformed with AGS8-C and delta AGS8-C in the pYES2-containing GAL1 promoter. The yeast strain was modified to grow without histidine on activation of G-protein. Induction (+): induction of translation of AGS8 domains by galactose. The representative of 4 independent experiments with similar results.
doi:10.1371/journal.pone.0091980.g003

Advantage of the AGS8-peptide for Targeted Disruption of the Gβγ Pathway

The data presented thus far indicated that the AGS8-peptide blocked the AGS8-Gβγ interaction and the signaling events the downstream of AGS8-Gβγ. We next asked whether inhibition of the Gβγ-mediated signal generally had a cardioprotective effect as was observed with the AGS8-peptide. Gallein is an inhibitor of Gβγ-mediated signaling that occupies a "common" interaction surface of Gβγ and inhibits the interaction of Gβγ-regulated proteins with Gβγ [25]. Thus, gallein is expected to block a wide range of Gβγ signals in cells, including CX43 regulation mediated by AGS-Gβγ. We previously demonstrated that gallein completely inhibits hypoxia-induced internalization of CX43 at 100 μM, as observed in the knockdown of AGS8, but not at 1 μM [13].

Here, we first examined the influence of the AGS8-peptide and gallein on the viability of cells. Cardiomyocytes were incubated with gallein for 24 h, and their viability was determined by MTT assay. Even the lowest concentration of gallein (1 μM) caused damage in the cardiomyocytes, indicating that broad inhibition of Gβγ did not have a protective effect (Fig. 7). In contrast, the AGS8-pepetide did not show cytotoxicity at 1 μM, the concentration that completely blocked the AGS8-Gβγ–mediated signal event. This suggests that the AGS8-peptide is a promising candidate for protection of cardiomyocytes from hypoxia-mediated apoptosis.

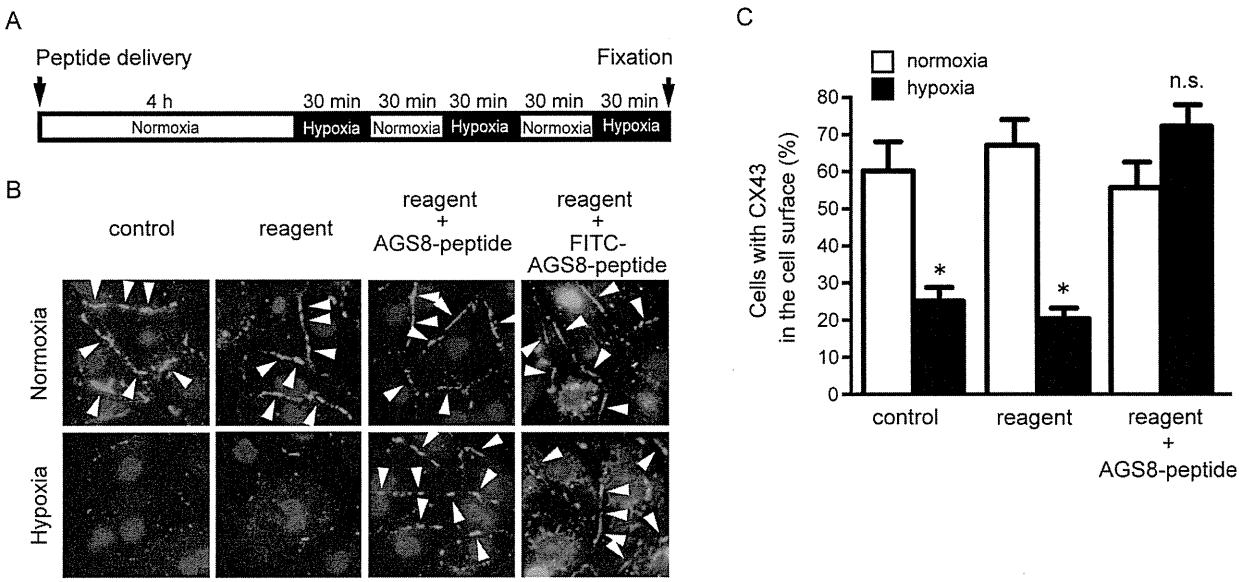

Figure 4. Effect of AGS8-peptide on localization of connexin 43 (CX43) of cultured cardiomyocytes. (A) Cardiomyocytes were exposed 3 times to 30 min of hypoxia (1% oxygen) intermittent with 30 min of reoxygenation 4 h after (without or with) transfection of AGS8-peptide (1 μM) or FITC-conjugated AGS8-peptide (1 μM). (B) Localization of CX43 in the cardiomyocytes under normoxia and hypoxia. The figures demonstrated in the triple color of CX43 (*red, arrow*), nuclei (DAPI, *blue*) and FITC-conjugated AGS8-peptide (*green*). The representative of 5 independent experiments with similar results. (C) The number of cardiomyocytes expressing CX43 in the cell surface were counted. Please note that ~ 90% cells were detectable at the point of fixation. Data are represent 170–260 cells from 5 of independent experiments. *, $p<0.05$ vs normoxia group.
doi:10.1371/journal.pone.0091980.g004

Discussion

AGS8-peptide, the sequence of which was derived from the amino-acid sequences of the Gβγ-binding domain of AGS8, blocked the association of AGS8 with Gβγ and inhibited AGS8-mediated events under hypoxia. Notably, AGS8-peptide inhibited the change in permeability of cell-surface CX43 and the apoptosis of cardiomyocytes. AGS8-peptide did not show cytotoxicity under normoxia, in contrast to the small molecule gallein, which produced deleterious effects by general inhibition of Gβγ-signaling. These data indicate that the AGS8-Gβγ complex plays a pivotal role in triggering the hypoxia-induced apoptosis of cardiomyocytes. Furthermore, they suggest an advantage of targeted disruption of G-protein signaling by the AGS-based peptide in protecting cardiomyocytes from hypoxia-induced apoptosis.

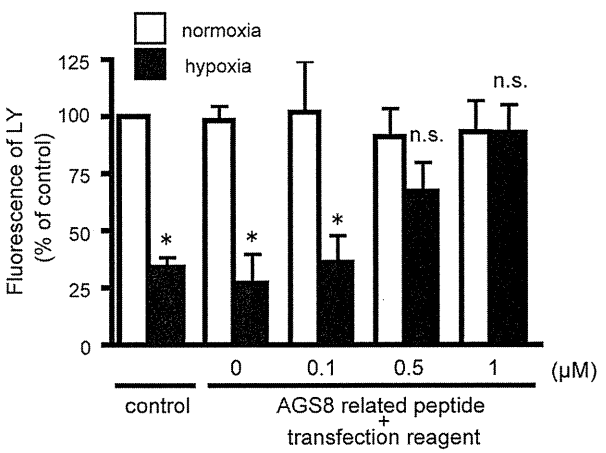

Figure 5. Uptake of connexin selective fluorescence dye, Lucifer Yellow (LY) to the cardiomyocytes. Cells were incubated with 1 mM of LY for 45 min in normal culture medium. Excess LY was removed and cells were rinsed with PBS. The fluorescence of LY was evaluated by inverted fluorescence microscope. The fluorescence of LY was quantified by the intensity of fluorescence of 10 randomly selected fields. The non-selective binding and/or incorporation of LY was determined fluorescence in the presence of a connexin hemichannel blocker, 50 μM of Lanthanum which was added 30 min prior to LY. *, $p<0.05$ vs cells in normoxia; *n.s.*, not statistically significant. N = 4 from 4 independent experiments.
doi:10.1371/journal.pone.0091980.g005

Several peptides have been developed to manipulate the broad signal initiated by accessory proteins for G-proteins. For example, an inhibitor of accessory proteins for heterotrimeric G-protein has been developed for RGS proteins. RGS proteins share 120–130 amino acids of an RGS-homology domain, which interact with the Gα subunit and accelerate GTPase activity [26,27]. RGS-peptides, which were designed on the basis of the X-ray structure of the Gαi switch I region of RGS4-Gαi, successfully modulate muscarinic receptor-regulated potassium currents in atrial myocytes [28]. RGS-peptides were initially designed to mimic the surface of G-protein to inhibit GAP activity, which produced the potential to suppress many events mediated by a variety of RGS proteins. As another example, a peptide, the sequence of which is based on G-protein regulatory (GPR) or GoLOCO motifs, is a cassette of 20–25 amino acids that stabilizes the GDP-bound conformation of Gα and clearly inhibits Gαi activation in vitro, suggesting its potential as an inhibitor of general Gαi signaling in cells [29].

Alternatively, the AGS8 peptide was designed on the basis of the AGS-Gβγ interface, with the objective of suppressing the specific signal evoked by AGS-Gβγ for all Gβγ signaling. It has been demonstrated that Gβγ-interacting proteins share an overlapping

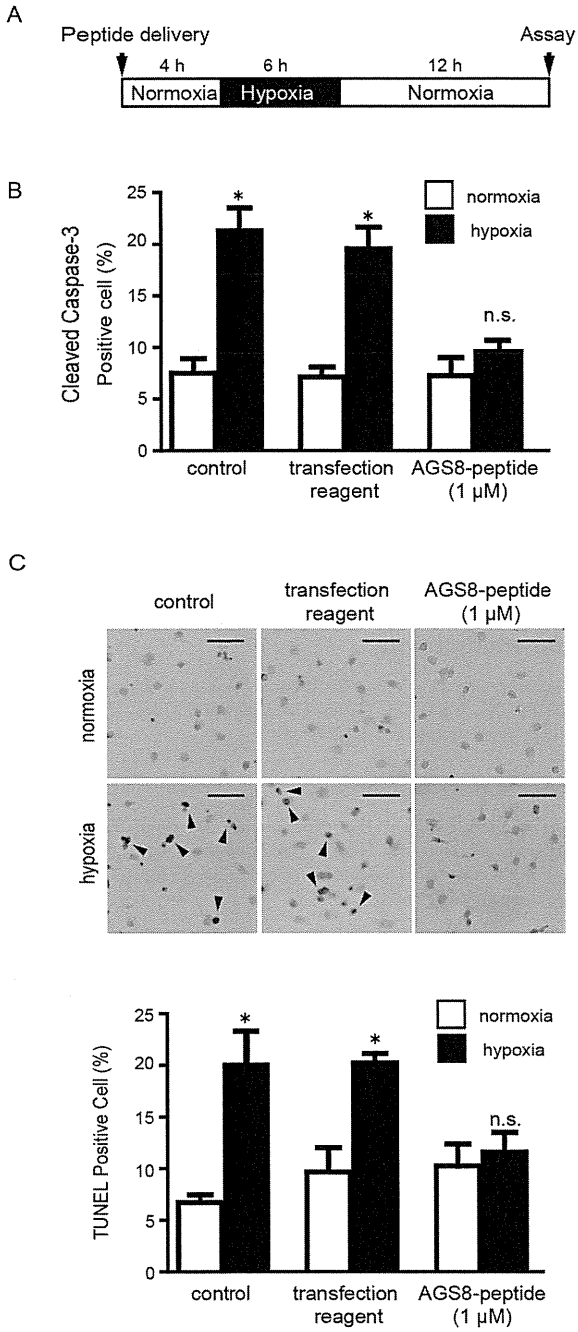

Figure 6. Effect of AGS8 peptide on hypoxia-induced apoptosis of cardiomyocytes. (A) Neonatal cardiomyocytes were exposed to hypoxia (1% oxygen) or normoxia as indicated duration without or with introduction of AGS8-peptide. Apoptosis was assessed by immunofluorescent detection of the active form of caspase-3 (cleaved caspase-3) (B) or TUNEL stain (C) as described in the experimental procedures. (C) Upper panel indicates representative apoptotic (*dark blue, arrow*) and non-apoptotic cells (*red*) after TUNEL staining. Scale bars indicate 100 μm. Approximately 3000 cells of 10 independent fields were counted for each experiments. A separate experiment indicated that AGS8-peptide did not influence the level of AGS8 within the 4-h treatment (1.0 μM peptide; 98.2±7.3% versus no reagent alone group, not statistically significant, $n=4$). *, $p<0.05$ vs cells in normoxia; *n.s.*, not statistically significant. N = 5 from 5 independent experiments.
doi:10.1371/journal.pone.0091980.g006

interface on the surface of Gβγ [30,31]. We previously demonstrated that the Gβγ-interacting surface of AGS8 includes the shared-site [32]. However, the entire Gβγ-interacting surface of AGS8 may include an additional interface, which is required to form an AGS8-specific signal complex. Our results indicated that 45 amino acids were required to evoke cell signaling by the AGS-Gβγ complex. The amino acid sequence of this domain did not have similarity to other known Gβγ interfaces [33–35], suggesting this sequence represents the AGS8-specifc interface that forms this particular complex. In fact, the AGS8-peptide designed to recognize this region successfully inhibited formation of the AGS8-Gβγ complex and subsequent cell events mediated by AGS8-Gβγ. However, currently, there is not enough information to determine whether the AGS8-peptide covers the common Gβγ interface or influences the interaction of Gβγ with other molecules. These issues are to be investigated elsewhere.

AGS-Gβγ–mediated signaling is required for hypoxia-induced apoptosis of cardiomyocytes [13]. Gβγ is known to conduct pro-apoptotic signaling via p38MAPK, JNK, or PLCβ, whereas anti-apoptotic signaling is also mediated by Gβγ via PI3K-Akt or ERK depending on type of cell and stimulus [36–39]. Although the involvement of these Gβγ-mediated pathways in the AGS-Gβγ pathway or other players in the AGS-Gβγ protein complex are yet to be determined, the current data indicate the presence of a critical signaling pathway mediated by the AGS8-Gβγ complex leading to apoptosis in cardiomyocytes.

The channel protein CX43 plays a role in the apoptotic process by regulating the permeability of small molecules, including adenosine 5′-triphosphate, adenosine diphosphate, adenosine, cAMP, inositol-1,4,5-triphosphate, glutamate, and glutathione [14,15,40–42]. In response to hypoxia, AGS8 organizes the complex that includes Gβγ, CX43, and possibly kinases that initiate phosphorylation of CX43 [13]. Multiple phosphorylation sites on CX43 are regulated by specific kinases under ischemic

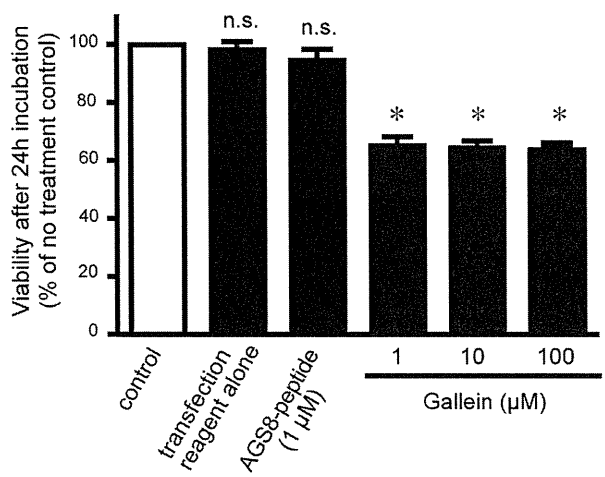

Figure 7. Effect of AGS8-peptide or Gallein on the viability of cardiomyocytes determined by MTT assay. Neonatal cardiomyocytes were cultured for 24 h with AGS8-peptide or Gallein. Gallein occupied a "common" interaction surface of Gβγ and inhibited its interaction with Gβγ-regulated proteins. *, $p<0.05$ vs cells in normoxia; *n.s.*, not statistically significant. N = 5 from 5 independent experiments.
doi:10.1371/journal.pone.0091980.g007

conditions, and each phosphorylation critically influences the permeability and localization of CX43 in the sarcolemma [43,44]. The inhibition of internalization of CX43 by AGS8-peptide may suggest that AGS8-peptide blocked the recruitment of components into the complex and/or phosphorylation of CX43 within the complex. AGS8 may play a role in separating the hypoxic/ischemic cardiomyocytes from healthy tissue by disconnecting the gap junction, which can contribute to arrhythmia and contraction failure during ischemia. Although the validity of this hypothesis is yet to be tested in confirmed or animal models, our observations support this possibility.

Myocardial ischemia activates multiple cascades that initiate intracellular ionic and chemical changes leading cell to death [17,18]. Although great efforts have been made over many years, therapeutic approaches to ischemic heart disease still need further development [45,46]. We previously demonstrated that AGS8-Gβγ signaling was activated under hypoxia and did not constitutively stimulate the apoptotic pathway, because the pro-apoptotic effects of AGS were not observed in cells cultured under normoxia [13]. In fact, AGS8-peptide effectively protected cardiomyocytes from hypoxia-mediated cell death, but did not cause cell damage under normoxia. Thus, AGS8-peptide has the potential to save a subpopulation of cardiomyocytes exposed to hypoxia without producing damage to the entire myocardium. This is an advantage of targeted disruption of specific signaling by AGS8-peptide, and it stands in contrast to the deleterious effects caused by general inhibition of Gβγ signaling with gallein.

Peptide-based reagents designed from the sequences of accessory proteins for heterotrimeric G-protein have potential to manipulate alternative signaling events distinct from GPCR-mediated G-protein signaling. At this stage, the potential of peptide-based reagents, including AGS8-peptide, remains limited by their ability to penetrate the membrane, their stability, and the modes of delivery available for their use as clinical drugs. The strategies for effective delivery of therapeutic peptides into the cell include conjugation with cell-penetrating peptides, incorporation into polymeric nanoparticles, and virus-mediated release of peptides [47–49]. Each strategy still has challenges with respect to the efficiency or selectivity of delivery as well as safety in healthy tissues or cells [47,49,50]. Although intracellular use of peptide targeting is not yet a common practice, delivery systems are continuously being developed, which will increase the potential for use of peptide-targeting therapy. We have demonstrated the possibility of regulating intracellular signaling mediated by accessory proteins for heterotrimeric G-protein, which could be a starting point for development of peptides or compounds to regulate AGS8-Gβγ signaling.

Targeted disruption of the interaction of G-protein with accessory proteins for heterotrimeric G-protein is a promising therapeutic strategy because these molecules mediate critical signaling distinct from the receptor-mediated pathway. In this study, we demonstrated that AGS8-peptide could be part of a novel therapeutic approach for the protection of ischemia in the heart that has enhanced specificity and fewer side effects. Although efforts to intervene in G-protein signaling have been focused on the interface of the GPCR-heterotrimeric G-protein, our data highlight the advantages of accessory proteins for heterotrimeric G-protein as alternative therapeutic targets in human diseases.

Acknowledgments

We acknowledge Dr. James R. Broach (Molecular Biology, Princeton University, NJ, USA) and Cadus Pharmaceutical Corp. (NY, USA) for providing yeast strains used in this study.

Author Contributions

Conceived and designed the experiments: M. Sato. Performed the experiments: M. Sato MH HS YY. Analyzed the data: M. Sakima AAM TF UY SO. Contributed reagents/materials/analysis tools: UY SO TF YI. Wrote the paper: M. Sato.

References

1. Birnbaumer L (2007) Expansion of signal transduction by G proteins. The second 15 years or so: from 3 to 16 alpha subunits plus betagamma dimers. Biochim Biophys Acta 1768: 772–793.
2. Sato M, Blumer JB, Simon V, Lanier SM (2006) ACCESSORY PROTEINS FOR G PROTEINS: Partners in Signaling. Annu Rev Pharmacol Toxicol 46: 151–187.
3. Blumer JB, Smrcka AV, Lanier SM (2007) Mechanistic pathways and biological roles for receptor-independent activators of G-protein signaling. Pharmacol Ther 113: 488–506.
4. Sjogren B (2011) Regulator of G protein signaling proteins as drug targets: current state and future possibilities. Adv Pharmacol 62: 315–347.
5. Sato M (2013) Roles of Accessory Proteins for Heterotrimeric G-Protein in the Development of Cardiovascular Diseases. Circ J.
6. Cismowski MJ, Ma C, Ribas C, Xie X, Spruyt M, et al. (2000) Activation of heterotrimeric G-protein signaling by a ras-related protein. Implications for signal integration. J Biol Chem 275: 23421–23424.
7. McGrath MF, Ogawa T, de Bold AJ (2012) Ras dexamethasone-induced protein 1 is a modulator of hormone secretion in the volume overloaded heart. Am J Physiol Heart Circ Physiol 302: H1826–1837.
8. Wieland T, Mittmann C (2003) Regulators of G-protein signalling: multifunctional proteins with impact on signalling in the cardiovascular system. Pharmacol Ther 97: 95–115.
9. Gu S, Cifelli C, Wang S, Heximer SP (2009) RGS proteins: identifying new GAPs in the understanding of blood pressure regulation and cardiovascular function. Clin Sci (Lond) 116: 391–399.
10. Zhang P, Mende U (2011) Regulators of G-protein signaling in the heart and their potential as therapeutic targets. Circ Res 109: 320–333.
11. Sato M, Hiraoka M, Suzuki H, Bai Y, Kurotani R, et al. (2011) Identification of transcription factor E3 (TFE3) as a receptor-independent activator of Galpha16: gene regulation by nuclear Galpha subunit and its activator. J Biol Chem 286: 17766–17776.
12. Sato M, Cismowski MJ, Toyota E, Smrcka AV, Lucchesi PA, et al. (2006) Identification of a receptor-independent activator of G protein signaling (AGS8) in ischemic heart and its interaction with Gbetagamma. Proc Natl Acad Sci U S A 103: 797–802.
13. Sato M, Jiao Q, Honda T, Kurotani R, Toyota E, et al. (2009) Activator of G protein signaling 8 (AGS8) is required for hypoxia-induced apoptosis of cardiomyocytes: role of G betagamma and connexin 43 (CX43). J Biol Chem 284: 31431–31440.
14. Harris AL (2007) Connexin channel permeability to cytoplasmic molecules. Prog Biophys Mol Biol 94: 120–143.
15. Rodriguez-Sinovas A, Cabestrero A, Lopez D, Torre I, Morente M, et al. (2007) The modulatory effects of connexin 43 on cell death/survival beyond cell coupling. Prog Biophys Mol Biol 94: 219–232.
16. Zhang SS, Shaw RM (2013) Multilayered regulation of cardiac ion channels. Biochim Biophys Acta 1833: 876–885.
17. Yellon DM, Hausenloy DJ (2007) Myocardial reperfusion injury. N Engl J Med 357: 1121–1135.
18. Bishopric NH, Andreka P, Slepak T, Webster KA (2001) Molecular mechanisms of apoptosis in the cardiac myocyte. Curr Opin Pharmacol 1: 141–150.
19. Sato M, Gettys TW, Lanier SM (2004) AGS3 and signal integration by Galpha(s)- and Galpha(i)-coupled receptors: AGS3 blocks the sensitization of adenylyl cyclase following prolonged stimulation of a Galpha(i)-coupled receptor by influencing processing of Galpha(i). J Biol Chem 279: 13375–13382.
20. Sato M, Ribas C, Hildebrandt JD, Lanier SM (1996) Characterization of a G-protein activator in the neuroblastoma-glioma cell hybrid NG108-15. J Biol Chem 271: 30052–30060.
21. Sato M, Ohsaki Y, Tobise K (1995) Transforming growth factor-beta 1 proliferated vascular smooth muscle cells from spontaneously hypertensive rats. Am J Hypertens 8: 160–166.
22. Thuc LC, Teshima Y, Takahashi N, Nagano-Torigoe Y, Ezaki K, et al. (2010) Mitochondrial K(ATP) channels-derived reactive oxygen species activate pro-survival pathway in pravastatin-induced cardioprotection. Apoptosis 15: 669–678.
23. Cismowski MJ, Takesono A, Ma C, Lizano JS, Xie X, et al. (1999) Genetic screens in yeast to identify mammalian nonreceptor modulators of G-protein signaling. Nat Biotechnol 17: 878–883.
24. Takesono A, Cismowski MJ, Ribas C, Bernard M, Chung P, et al. (1999) Receptor-independent activators of heterotrimeric G-protein signaling pathways. J Biol Chem 274: 33202–33205.

25. Lehmann DM, Seneviratne AM, Smrcka AV (2008) Small molecule disruption of G protein beta gamma subunit signaling inhibits neutrophil chemotaxis and inflammation. Mol Pharmacol 73: 410–418.
26. Sjogren B, Blazer LL, Neubig RR (2010) Regulators of G protein signaling proteins as targets for drug discovery. Prog Mol Biol Transl Sci 91: 81–119.
27. Kimple AJ, Bosch DE, Giguere PM, Siderovski DP (2011) Regulators of G-protein signaling and their Galpha substrates: promises and challenges in their use as drug discovery targets. Pharmacol Rev 63: 728–749.
28. Roof RA, Jin Y, Roman DL, Sunahara RK, Ishii M, et al. (2006) Mechanism of action and structural requirements of constrained peptide inhibitors of RGS proteins. Chem Biol Drug Des 67: 266–274.
29. Peterson YK, Bernard ML, Ma H, Hazard S 3rd, Graber SG, et al. (2000) Stabilization of the GDP-bound conformation of Gialpha by a peptide derived from the G-protein regulatory motif of AGS3. J Biol Chem 275: 33193–33196.
30. Ford CE, Skiba NP, Bae H, Daaka Y, Reuveny E, et al. (1998) Molecular basis for interactions of G protein betagamma subunits with effectors. Science 280: 1271–1274.
31. Smrcka AV (2008) G protein betagamma subunits: Central mediators of G protein-coupled receptor signaling. Cell Mol Life Sci 65: 2191–2214.
32. Yuan C, Sato M, Lanier SM, Smrcka AV (2007) Signaling by a non-dissociated complex of G Protein betagamma and alpha subunits stimulated by a receptor-independent activator of G protein signaling, AGS8. J Biol Chem 282: 19938–19947.
33. Touhara K, Inglese J, Pitcher JA, Shaw G, Lefkowitz RJ (1994) Binding of G protein beta gamma-subunits to pleckstrin homology domains. J Biol Chem 269: 10217–10220.
34. Chen J, DeVivo M, Dingus J, Harry A, Li J, et al. (1995) A region of adenylyl cyclase 2 critical for regulation by G protein beta gamma subunits. Science 268: 1166–1169.
35. Qin N, Platano D, Olcese R, Stefani E, Birnbaumer L (1997) Direct interaction of gbetagamma with a C-terminal gbetagamma-binding domain of the Ca2+ channel alpha1 subunit is responsible for channel inhibition by G protein-coupled receptors. Proc Natl Acad Sci U S A 94: 8866–8871.
36. New DC, Wu K, Kwok AW, Wong YH (2007) G protein-coupled receptor-induced Akt activity in cellular proliferation and apoptosis. FEBS J 274: 6025–6036.
37. Goldsmith ZG, Dhanasekaran DN (2007) G protein regulation of MAPK networks. Oncogene 26: 3122–3142.
38. Marinissen MJ, Gutkind JS (2001) G-protein-coupled receptors and signaling networks: emerging paradigms. Trends Pharmacol Sci 22: 368–376.
39. Adams JW, Brown JH (2001) G-proteins in growth and apoptosis: lessons from the heart. Oncogene 20: 1626–1634.
40. Shintani-Ishida K, Uemura K, Yoshida K (2007) Hemichannels in cardiomyocytes open transiently during ischemia and contribute to reperfusion injury following brief ischemia. Am J Physiol Heart Circ Physiol 293: H1714–1720.
41. Solan JL, Marquez-Rosado L, Sorgen PL, Thornton PJ, Gafken PR, et al. (2007) Phosphorylation at S365 is a gatekeeper event that changes the structure of Cx43 and prevents down-regulation by PKC. J Cell Biol 179: 1301–1309.
42. Bao X, Lee SC, Reuss L, Altenberg GA (2007) Change in permeant size selectivity by phosphorylation of connexin 43 gap-junctional hemichannels by PKC. Proc Natl Acad Sci U S A 104: 4919–4924.
43. Ek-Vitorin JF, King TJ, Heyman NS, Lampe PD, Burt JM (2006) Selectivity of connexin 43 channels is regulated through protein kinase C-dependent phosphorylation. Circ Res 98: 1498–1505.
44. Lampe PD, Cooper CD, King TJ, Burt JM (2006) Analysis of Connexin43 phosphorylated at S325, S328 and S330 in normoxic and ischemic heart. J Cell Sci 119: 3435–3442.
45. Windecker S, Bax JJ, Myat A, Stone GW, Marber MS (2013) Future treatment strategies in ST-segment elevation myocardial infarction. Lancet 382: 644–657.
46. Jneid H (2012) The 2012 ACCF/AHA Focused Update of the Unstable Angina/Non-ST-Elevation Myocardial Infarction (UA/NSTEMI) Guideline: a critical appraisal. Methodist Debakey Cardiovasc J 8: 26–30.
47. Clemons TD, Viola HM, House MJ, Iyer KS, Hool LC (2013) Examining efficacy of "TAT-less" delivery of a peptide against the L-type calcium channel in cardiac ischemia-reperfusion injury. ACS Nano 7: 2212–2220.
48. Flores-Munoz M, Godinho BM, Almalik A, Nicklin SA (2012) Adenoviral delivery of angiotensin-(1–7) or angiotensin-(1–9) inhibits cardiomyocyte hypertrophy via the mas or angiotensin type 2 receptor. PLoS One 7: e45564.
49. Svensen N, Walton JG, Bradley M (2012) Peptides for cell-selective drug delivery. Trends Pharmacol Sci 33: 186–192.
50. Jones AT, Sayers EJ (2012) Cell entry of cell penetrating peptides: tales of tails wagging dogs. J Control Release 161: 582–591.

J Physiol Sci (2014) 64:177–183
DOI 10.1007/s12576-014-0309-8

ORIGINAL PAPER

Hyperthermia generated with ferucarbotran (Resovist®) in an alternating magnetic field enhances cisplatin-induced apoptosis of cultured human oral cancer cells

Itaru Sato · Masanari Umemura · Kenji Mitsudo · Mitomu Kioi · Hideyuki Nakashima · Toshinori Iwai · Xianfeng Feng · Kayoko Oda · Akiyoshi Miyajima · Ayako Makino · Maki Iwai · Takayuki Fujita · Utako Yokoyama · Satoshi Okumura · Motohiko Sato · Haruki Eguchi · Iwai Tohnai · Yoshihiro Ishikawa

Received: 27 January 2014 / Accepted: 20 February 2014 / Published online: 12 March 2014

Abstract Hyperthermia is a promising anti-cancer treatment in which the tissue temperature is increased to 42–45 °C, and which is often used in combination with chemotherapy or radiation therapy. Our aim in the present work was to examine the feasibility of combination therapy for oral cancer with cisplatin and hyperthermia generated with ferucarbotran (Resovist®; superparamagnetic iron oxide) in an alternating magnetic field (AMF). First, we established that administration of ferucarbotran at the approved dosage for magnetic resonance imaging provides an iron concentration sufficient to increase the temperature to 42.5 °C upon exposure to AMF. Then, we examined the effect of cisplatin combined with ferucarbotran/AMF-induced hyperthermia on cultured human oral cancer cells (HSC-3 and OSC-19). Cisplatin alone induced apoptosis of cancer cells in a dose-dependent manner, as is well known. However, the combination of cisplatin with ferucarbotran/AMF was significantly more effective than cisplatin alone. This result suggests that it might be possible to reduce the clinically effective dosage of cisplatin by administering it in combination with ferucarbotran/AMF-induced hyperthermia, thereby potentially reducing the incidence of serious cisplatin-related side effects. Further work seems justified to evaluate simultaneous thermo-chemotherapy as a new approach to anticancer therapy.

Keywords Ferucarbotran · Hyperthermia · Oral cancer · Anti-cancer effect · Cisplatin · Resovist®

Abbreviations

AMF	Alternating magnetic field
MNPs	Magnetic nanoparticles
MRI	Magnetic resonance imaging
SPIO	Superparamagnetic iron oxide

Introduction

Cancer cells are more vulnerable to increased temperature than normal cells [1]. Thus, hyperthermia is viewed as a promising approach in cancer therapy [2]. Many techniques have been reported to increase the temperature of cancer tissues, such as whole-body hyperthermia [3], radiofrequency hyperthermia [4], microwave-induced hyperthermia [5], and implantable needles [6]. However, with all

I. Sato · M. Umemura (✉) · X. Feng · K. Oda · A. Miyajima · A. Makino · M. Iwai · T. Fujita · U. Yokoyama · Y. Ishikawa (✉)
Cardiovascular Research Institute, Yokohama City University, Graduate School of Medicine, 3-9 Fukuura, Yokohama 236-0004, Japan
e-mail: umemurma@yokohama-cu.ac.jp

Y. Ishikawa
e-mail: yishikaw@med.yokohama-cu.ac.jp

I. Sato · K. Mitsudo · M. Kioi · H. Nakashima · T. Iwai · I. Tohnai
Department of Oral and Maxillofacial Surgery, Yokohama City University Graduate School of Medicine, 3-9 Fukuura, Yokohama 236-0004, Japan

S. Okumura
Tsurumi University School of Dental Medicine, Tsurumi 230-8501, Japan

M. Sato
Department of Physiology, Aichi Medical University, Nagakute 480-1195, Aichi, Japan

H. Eguchi
Advanced Applied Science Department, Research Laboratory, IHI Corporation, Yokohama 235-8501, Japan

these modalities, it remains difficult to increase the temperature of only the cancer tissues in a controlled manner without damaging surrounding normal tissues.

More than 40,000 people are diagnosed with oral cancer, including cancers of the mouth, tongue, tonsils, and throat, every year in the US alone. Oral cancer can cause functional damage and disfigurement, and, in its advanced stages, it invades surrounding organs, causing disorders of speech, swallowing, and even chewing. Surgery may have serious adverse effects, so chemotherapy or radiation therapy is often favored in oral cancer patients, not with standing potentially serious systemic side effects. Hyperthermia is often preferred, e.g., for metastatic N3 cervical lymph nodes, because it has fewer adverse side effects. However, it is difficult to induce hyperthermia in a metastatic node-specific manner. Nevertheless, selective hyperthermia has been studied as a possible approach to obtain tumor-specific cytotoxicity, e.g., by ferromagnetic embolization [7]. More recently, magnetic nanoparticles (MNPs) have been investigated for this purpose, because MNPs generate heat when they are exposed to an alternating magnetic field (AMF) as a result of hysteresis and relaxational losses [8].

Ferucarbotran (Resovist®) is an organ-specific contrast agent used in magnetic resonance imaging (MRI) of local tumors, and the permissible dose in humans has been established by at least two studies [9, 10]. Because ferucarbotran consists of superparamagnetic iron oxide (SPIO) coated with carboxydextran, it generates heat when it is exposed to an AMF [11, 12], and it has been reported to induce selective hyperthermia when used in arterial embolization [11]. However, it has not been established whether ferucarbotran is suitable for inducing hyperthermia in cancer treatment.

Cisplatin (*cis*-diaminedichloroplatinum II; CDDP) is widely used in chemotherapy in many types of cancer, including oral cancers [13]. However, it has serious side effects, including acute kidney damage and/or renal failure [14–16]. Recent studies have demonstrated that hyperthermia stimulates cellular uptake of cisplatin [17, 18] and consequently enhances the cytotoxicity of cisplatin in cancer cells, both in vitro and in vivo [19–21]. Thus, combined treatment with cisplatin plus hyperthermia may allow the effective dose of cisplatin to be decreased sufficiently to minimize serious side effects.

Accordingly, in order to examine the feasibility of using combination therapy with cisplatin and ferucarbotran/AMF-induced hyperthermia in the therapy of oral cancer, in this study we examined the effect of the combined treatment on oral cancer cells in culture. Our results confirmed that ferucarbotran/AMF-induced hyperthermia significantly enhances the effect of cisplatin. Because both cisplatin and ferucarbotran have already been approved for clinical use, early introduction of this technique, at least for oral cancers, should be feasible.

Materials and methods

Reagent, drug and cell lines

Ferucarbotran (Resovist®) was purchased from FUJIFILM Pharma (Tokyo, Japan) [11]. Cisplatin was purchased from Wako Pure Chemical Industries (Osaka, Japan). Human oral squamous cell carcinoma cell lines OSC-19 and HSC-3 were purchased from the Japan Health Sciences Foundation, Health Science Research Resources Bank (Osaka, Japan). In all cases, cells from early passage cultures were stored and used for the experiments. OSC-19 and HSC-3 were cultured in Dulbecco's modified Eagle's medium (DMEM), 1 % penicillin–streptomycin, and 1 % L-glutamine.

Thermography

Thermal images were taken using a thermograph (infrared thermal imaging camera InfReC R300SR; Nippon Avionics, Tokyo, Japan). Temperature was also measured using a thermograph.

Alternating magnetic field (AMF) generator

An AMF was generated by a vertical coil with an inner diameter of 6.5 cm, driven by a transistor inverter (HOT SHOT; Ameritherm, New York, USA) operated at a

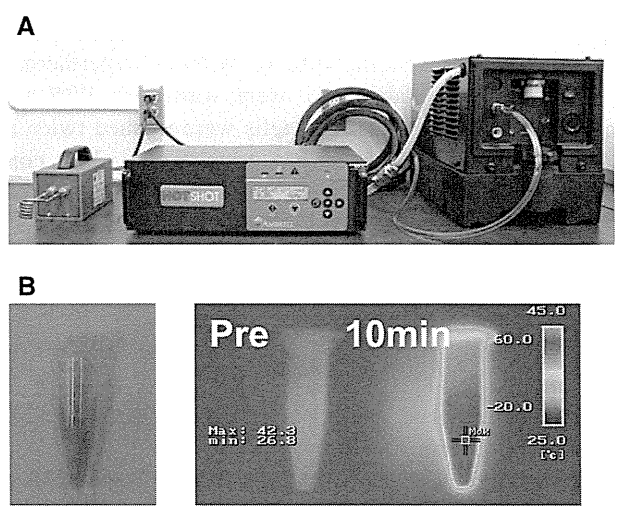

Fig. 1 Heat generation by ferucarbotran in an alternating magnetic field (AMF). **a** The alternating magnetic field (AMF) generator, **b** a photograph of ferucarbotran in medium (*left*), and thermal images of ferucarbotran in medium before (*middle*), and 10 min after AMF (308 kHz, EC 270 A) (*right*)

frequency of 308 kHz and electric current (EC) 250 A [12, 22–26]. Temperature was measured using a hand-held thermometer, HA-200 (Anritsu Meter, Tokyo, Japan).

Apoptosis assay

HSC-3 cells and OSC-19 (6×10^4 cells/well) were seeded on 6-cm dishes and incubated for 24 h. Cisplatin was then added to a concentration of 0 μM (control), 7.5 or 15 μM. When hyperthermia was to be applied, 10 mM ferucarbotran was added and AMF was performed with a HOT SHOT under the conditions described above [22, 25, 26]. Incubation was continued for 12 h at 37 °C, in an atmosphere of 5 % CO_2 in air. Cells were washed twice with cold PBS and suspended in 1× binding buffer at a concentration of 1×10^6 cells/ml. Next, a 100-μl aliquot of the solution, containing 1×10^5 cells, was transferred to a 5-ml culture tube. Then, 5 μl of allophycocyanin (APC) Annexin V and 5 μl of 7-aminoactinomycin D (AAD) (BD Biosciences, CA, USA) [27] were added to the tube. Incubation was continued for 15 min at room temperature (25 °C) in the dark. Finally, 400 μl of 1× binding buffer were added to each tube. Cells were examined by flow cytometry (BD FACSCanto II; BD Biosciences).

Cell cycle analysis

Cell cycle analysis was performed using The Cycletest™ Plus DNA Reagent Kit (BD Biosciences) according to the manufacturer's protocol [28]. Briefly, HCS-3 and OSC-19 cells treated with 0 μM (control), 7.5 or 15 μM cisplatin, with or without hyperthermia (10 mM ferucarbotan/AMF), were washed in PBS and fixed in 90 % ethanol. Fixed cells were washed twice in PBS and stained with 50 μM propidium iodide containing 5 μg/ml DNase-free RNase for 1 h, then analyzed by flow cytometry using a FACScan (BD FACSCanto II).

Statistical analysis

Data were analyzed using BD FACSDiva software (BD Biosciences). Data are expressed as mean ± SEM. Data were analyzed by one-way ANOVA followed by the Tukey post hoc test using GraphPad Prism software (GraphPad Software, CA, USA). The criterion of statistical significance was set at $p < 0.05$.

Results

Heat generation by ferucarbotran in an alternating magnetic field (AMF)

Heat production is determined by the magnetic properties of ferucarbotran, its concentration, and the strength of the AMF [12]. Therefore, we examined the heating effect of AMF on medium containing ferucarbotran by thermography (Fig. 1b). As shown in Fig. 2, the temperature increased time-dependently, and the extent of the increase was dependent on the concentration of ferucarbotran (Fig. 2a) and the magnitude of the EC used to generate AMF (Fig. 2b). The results showed that AMF produced at

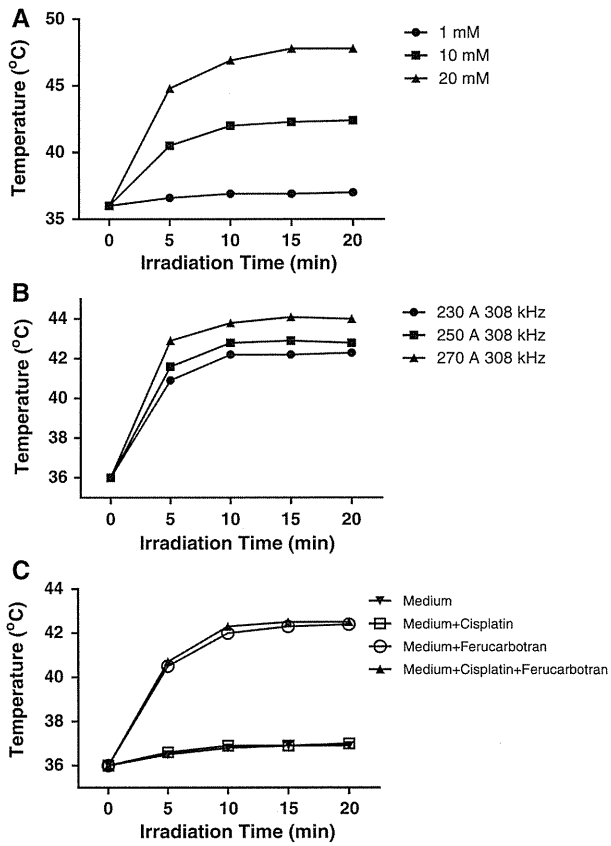

Fig. 2 Dependence of heat generation on ferucarbotran concentration and alternating magnetic field (AMF) strength. **a** Temperature–time curves at different concentrations of ferucarbotran (1, 10, or 20 mM equivalent of iron) on AMF at 308 kHz and EC 230 A. **b** Temperature–time curves in the presence of 10 mM ferucarbotran on AMF at different levels of electric current (230–270 A) at 308 kHz. **c** Effect of cisplatin (30 μM) on ferucarbotran (1, 10, or 20 mM equivalent of iron)/AMF (308 kHz, EC 230 A)-induced increase of temperature; medium only, medium + cisplatin, medium + ferucarbotran, and medium + cisplatin + ferucarbotran

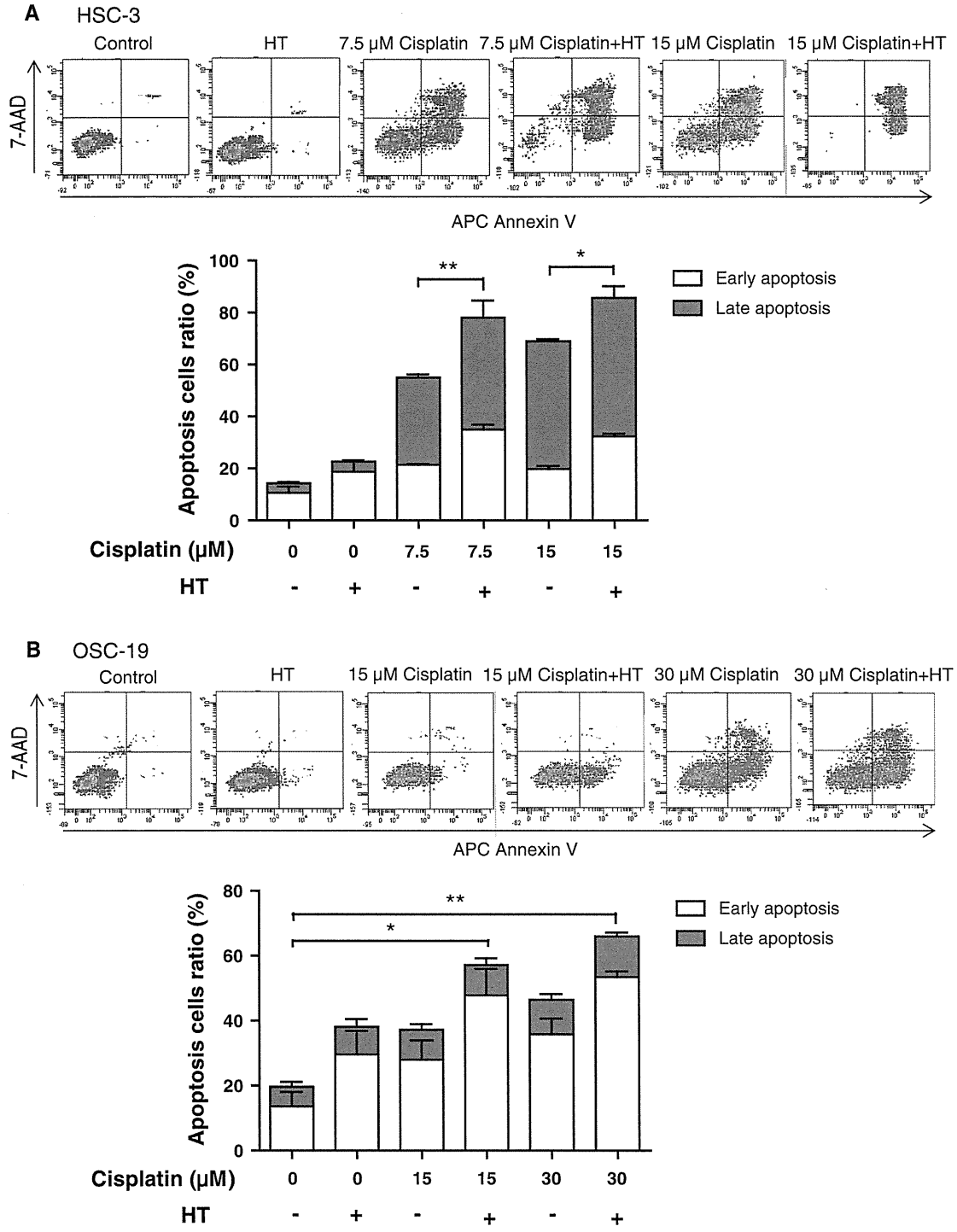

Fig. 3 Ferucarbotran/AMF-induced hyperthermia enhances the pro-apoptotic effect of cisplatin in human oral cancer cells. Annexin-V/PI staining of human oral cancer cells at 12-h intervals after treatment with 0, 7.5, or 15 μM cisplatin with or without hyperthermia (HT) in HSC-3 cells, and 0, 15, 30 μM cisplatin with or without HT in OSC-19 cells. **a** Representative analysis of apoptosis of HCS-3 cells and OSC-19 cells exposed to cisplatin and ferucarbotran with or without AMF. Annexin-V/PI method with FACS scan dot plot analysis was used to divide the treated and control cells into four groups: (1) living cells (*lower left quadrant*); (2) necrotic cells (*upper left quadrant*); (3) early apoptotic cells (*lower right quadrant*); and (4) late apoptotic cells (*upper right quadrant*). **b** Representative analysis of apoptosis of OSC-19 cells exposed to cisplatin with or without AMF. $*p < 0.05$, $**p < 0.01$; $n = 4$

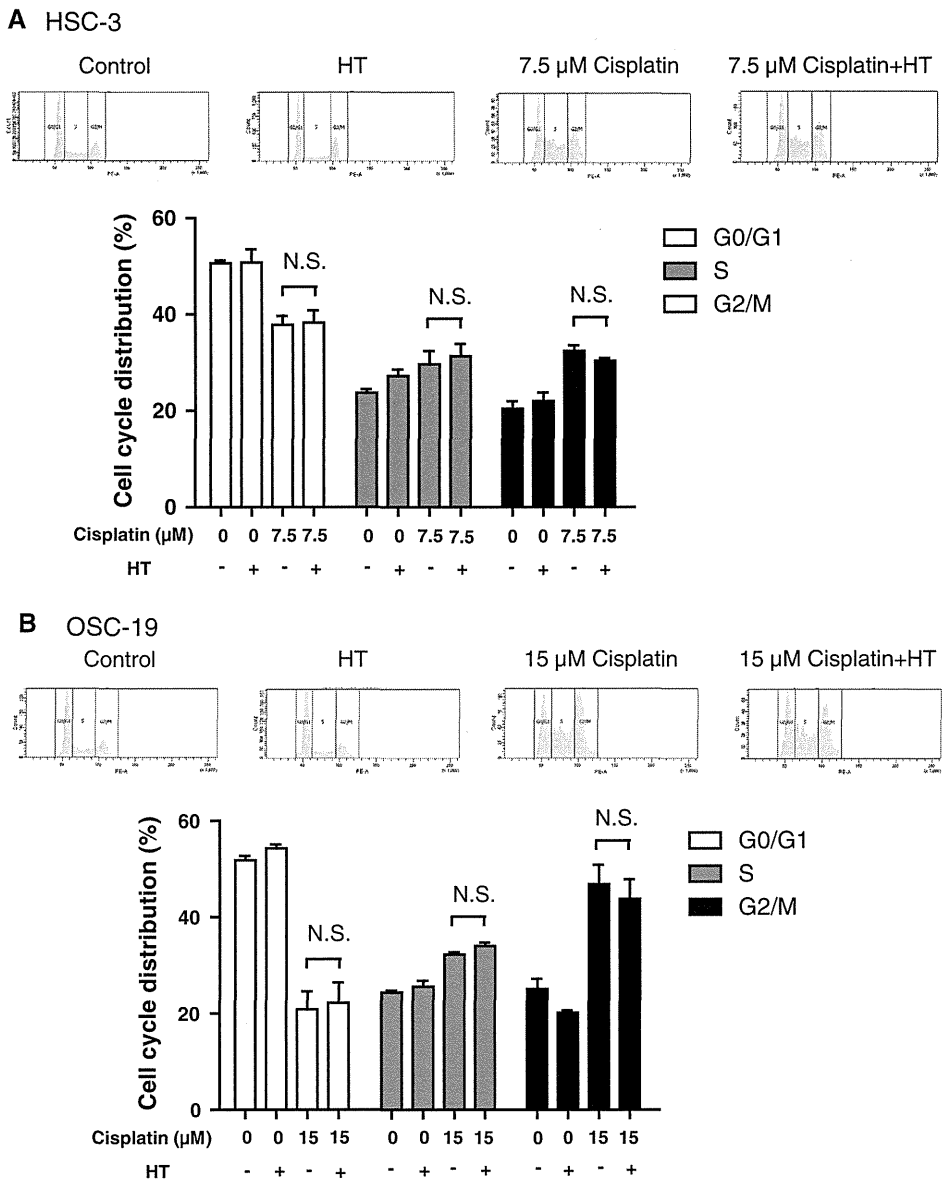

Fig. 4 Combination of cisplatin and ferucarbotran/AMF-induced hyperthermia causes G2/M arrest. Cell cycle analysis of HSC-3 and OSC-19 cells at 48-h intervals after treatment with 0, 7.5, or 15 μM of cisplatin with or without hyperthermia (HT). **a** Representative cell cycle analysis of HSC-3 cells in response to cisplatin treatment with or without AMF (*upper panel*) and of OSC-19 cells in response to cisplatin treatment with or without AMF (*lower panel*). *NS* not significant; $n = 4$

generator settings of 308 kHz and EC 250 A in the presence of 10 mM (equivalent of iron) ferucarbotran was sufficient to generate a temperature of 42.5 °C, and we adopted these conditions for the subsequent assays. We confirmed that cisplatin did not alter the heating effect under these conditions (Fig. 2c).

Ferucarbotran-enhanced cisplatin-mediated apoptosis

It has been reported that cisplatin induces apoptosis in cancer cells [29]. We thus examined whether ferucarbotran/AMF-induced hyperthermia further increased cisplatin-induced apoptosis in oral cancer cells. FACS analysis demonstrated that cisplatin increased both early and late apoptosis in a dose-dependent manner in HSC-3 cells (Fig. 3a) and OSC-19 cells (Fig. 3b). Ferucarbotran/AMF-induced hyperthermia for an hour significantly increased the apoptotic effect of cisplatin.

Cisplatin-induced G2/M arrest of human oral cancer cells was unaffected by hyperthermia

To examine whether hyperthermia modifies the mechanism of anti-cancer action of cisplatin, flow-cytometric cell-cycle analysis of treated cells was performed. Cisplatin induced potent G2/M arrest in both HSC-3 cells (Fig. 4a) and OSC-19 cells (Fig. 4b). We found that ferucarbotran/AMF-induced hyperthermia did not alter the effect of

cisplatin on the cell cycle. Thus, hyperthermia per se had no effect on the anti-cancer mechanism of cisplatin.

Discussion

Ferucarbotran is an organ-specific superparamagnetic contrast agent used in MRI, and its safety and maximum dosage (10 mM; 0.016 mL/kg, which contains 8 μmol (0.45 mg) Fe/kg equivalent of iron [30]) have been well established [9, 10]. Since hyperthermia has already been shown to enhance the anti-cancer effect of cisplatin [31] in the treatment of oral cancer, we anticipated that combination therapy with cisplatin and ferucarbotran/AMF-induced hyperthermia might be suitable for oral cancer treatment, making it possible to reduce the necessary dose of cisplatin and consequently reduce the risk of serious side effects.

Hyperthermia to induce apoptosis of cancer cells is best performed at about 42 °C, because temperatures above 44 °C have been reported to cause necrosis and damage to surrounding normal tissues [32]. Therefore, we first confirmed that the above concentration of ferucarbotran was sufficient to maintain a temperature of 42.5 °C under appropriate AMF conditions, and this level of hyperthermia could induce apoptosis of oral cancer cells, as evaluated by FACS analysis. It should be noted that it would still be necessary to optimize AMF conditions for clinical treatment. Similarly, it would be desirable to deliver cisplatin and ferucarbotran to oral cancer tissue in a selective manner. This may be achieved by the use of superselective intra-arterial infusion with a catheter, as we previously reported in oral cancer patients [33].

We previously reported that ROS production was higher in cancer cells than in normal cells, and was further increased when the temperature was increased [34]. Cisplatin also increases ROS production, and this is most likely the mechanism responsible for its anti-cancer effect [34, 35]. We confirmed that the combination of cisplatin and ferucarbotran/AMF-induced hyperthermia further enhanced ROS production (data not shown). This is important, because cisplatin may cause ototoxicity [36], so it is desirable to minimize the necessary cisplatin dose, as far as is consistent with therapeutic effectiveness, in the clinical context.

It is well known that cisplatin causes accumulation of cells in S phase and blocks the G0/G1 phases in xenografted human head and neck carcinoma cells [37], leading to apoptosis. [38, 39]. Our data showed that ferucarbotran/AMF-induced hyperthermia enhanced the anti-cancer effect of cisplatin without altering its characteristic effect on the cell cycle. Accordingly, ferucarbotran/AMF-induced hyperthermia did not appear to modify the mechanism of action of cisplatin in human oral cancer cells. Because both cisplatin and ferucarbotran are already in clinical use, we believe the combination of cisplatin with ferucarbotran/AMF-induced hyperthermia has the potential for early clinical application. It should at least be possible to reduce the clinically effective dosage of cisplatin by administering it in combination with ferucarbotran/AMF, thereby reducing the risk of serious cisplatin-related side effects. Further investigation seems warranted to confirm the safety and effectiveness of this combined treatment for oral cancers in humans.

Acknowledgments The authors are grateful to Akane Nagasako for technical assistance in this study. This work was supported in part by the Japan Society for the Promotion of Science (JSPS) (IS), as well as a Grant-in-Aid for JSPS Fellows (I.S.) from the Ministry of Health, Labor and Welfare of Japan (Y.I.), a Grant-in-Aid from the New Energy and Industrial Technology Development Organization of Japan (NEDO) (Y.I.), a Grant-in-Aid for Scientific Research on Innovative Areas (22136009) (Y.I.) from the Japanese Ministry of Education, Culture, Sports, Science, and Technology of Japan (Y.I.), a grant from the IHI Corporation (H.E.), and a Grant for a Research and Development Project of Yokohama City University (Y.I.).

Conflict of interest The authors declare no potential conflicts of interest.

References

1. van der Zee J (2002) Heating the patient: a promising approach? Ann Oncol 13(8):1173–1184
2. Abe M, Hiraoka M, Takahashi M, Egawa S, Matsuda C, Onoyama Y, Morita K, Kakehi M, Sugahara T (1986) Multi-institutional studies on hyperthermia using an 8-MHz radiofrequency capacitive heating device (Thermotron RF-8) in combination with radiation for cancer therapy. Cancer 58(8):1589–1595
3. Baba H, Clifton Stephens L, Strebel FR, Siddik ZH, Newman RA, Ohno S, Bull JMC (1991) Protective Effect of ICRF-187 against normal tissue injury induced by Adriamycin in combination with whole body hyperthermia. Cancer Res 51(13):3568–3577
4. Ikeda NHO, Kameda H, Ito H, Matsuda T (1994) Experimental study on thermal damage to dog normal brain. Int J Hyperth 10(4):553–561
5. Lin JCWY (1987) Interstitial microwave antennas for thermal therapy. Int J Hyperth 3(1):37–47
6. Stauffer PR, Cetas TC, Fletcher AM, Deyoung DW, Dewhirst MW, Oleson JR, Roemer RB (1984) Observations on the use of ferromagnetic implants for inducing hyperthermia. Biomed Eng, IEEE Trans 31(1):76–90
7. Barry JW, Bookstein JJ, Alksne JF (1981) Ferromagnetic embolization. Experimental evaluation. Radiology 138(2):341–349
8. Rosensweig RE (2002) Heating magnetic fluid with alternating magnetic field. J Magn Magn Mater 252:370–374
9. Reimer P, Balzer T (2003) Ferucarbotran (Resovist): a new clinically approved RES-specific contrast agent for contrast-enhanced MRI of the liver: properties, clinical development, and applications. Eur Radiol 13(6):1266–1276
10. Hamm BST, Taupitz M, Maibauer R, Speidel A, Huppertz A, Frenzel T, Lawaczeck R, Wolf KJ, Lange L (1994) Contrast-enhanced MR imaging of liver and spleen: first experience in humans with a new superparamagnetic iron oxide. J Magn Reson Imaging 4(5):659–668

11. Takamatsu S, Matsui O, Gabata T, Kobayashi S, Okuda M, Ougi T, Ikehata Y, Nagano I, Nagae H (2008) Selective induction hyperthermia following transcatheter arterial embolization with a mixture of nano-sized magnetic particles (ferucarbotran) and embolic materials: feasibility study in rabbits. Radiat Med 26(4):179–187
12. Murase K, Oonoki J, Takata H, Song R, Angraini A, Ausanai P, Matsushita T (2011) Simulation and experimental studies on magnetic hyperthermia with use of superparamagnetic iron oxide nanoparticles. Radiol Phys Technol 4(2):194–202
13. Fram RJ (1992) Cisplatin and platinum analogues: recent advances. Curr Opin Oncol 4(6):1073–1079
14. Arany I, Safirstein RL (2003) Cisplatin nephrotoxicity. Semin Nephrol 23(5):460–464
15. Meyer KBMN (1994) Cisplatin nephrotoxicity. Min Electrolyte Metab 20(4):201–213
16. Pabla N, Dong Z (2008) Cisplatin nephrotoxicity: mechanisms and renoprotective strategies. Kidney Int 73(9):994–1007
17. Los G, Van Vugt MJH, Den Engelse L, Pinedo HM (1993) Effects of temperature on the interaction of cisplatin and carboplatin with cellular DNA. Biochem Pharmacol 46(7):1229–1237
18. Los G, van Vugt MJ, Pinedo HM (1994) Response of peritoneal solid tumours after intraperitoneal chemohyperthermia treatment with cisplatin or carboplatin. Br J Cancer 69(2):235–241
19. Barlogie B, Corry PM, Drewinko B (1980) In vitro thermochemotherapy of human colon cancer cells with *cis*-dichlorodiammineplatinum(II) and mitomycin C. Cancer Res 40(4):1165–1168
20. Cohen JD, Robins HI (1987) Hyperthermic enhancement of *cis*-Diammine-1,1-cyclobutane dicarboxylate platinum(II) cytotoxicity in human leukemia cells in vitro. Cancer Res 47(16): 4335–4337
21. Los GSP, Wondergem J, Mutsaers PH, Havemen J, ten Bokkel Huinink D, Smals O, Gonzalez-Gonzalez D, McVie JG (1991) Optimisation of intraperitoneal cisplatin therapy with regional hyperthermia in rats. Eur J Cancer 27(4):472–477
22. Wang X, Chen Y, Huang C, Wang X, Zhao L, Zhang X, Tang J (2013) Contribution of a 300 kHz alternating magnetic field on magnetic hyperthermia treatment of HepG2 cells. Bioelectromagnetics 34(2):95–103
23. Zhao QLW, Cheng R, Mao L, Arnold RD, Howerth EW, Chen ZG, Platt S (2012) Magnetic nanoparticle-based hyperthermia for head and neck cancer in mouse models. Theranostics 2(1):113–121
24. Atsumi T, Jeyadevan B, Sato Y, Tohji K (2007) Heating efficiency of magnetite particles exposed to AC magnetic field. J Magn Magn Mater 310(2):2841–2843
25. Hayashi KNM, Sakamoto W, Yogo T, Miki H, Ozaki S, Abe M, Matsumoto T, Ishimura K (2013) Superparamagnetic nanoparticle clusters for cancer theranostics combining magnetic resonance imaging and hyperthermia treatment. Theranostics 3(6):366–376
26. Nakao KOY, Akao Y, Ito Y, Marukawa O, Tachibana S, Kawakami M, Sasaki S (2000) The synergistic effects of hyperthermia and anticancer drugs on induction of apoptosis. Med Electron Microsc 33(1):44–50
27. Shao Y, Aplin AE (2010) Akt3-mediated resistance to apoptosis in B-RAF–targeted melanoma cells. Cancer Res 70(16): 6670–6681
28. Lee JT, Li L, Brafford PA, van den Eijnden M, Halloran MB, Sproesser K, Haass NK, Smalley KSM, Tsai J, Bollag G et al (2010) PLX4032, a potent inhibitor of the B-Raf V600E oncogene, selectively inhibits V600E-positive melanomas. Pigment Cell Melanoma Res 23(6):820–827
29. Al-Bahlani S, Fraser M, Wong AYC, Sayan BS, Bergeron R, Melino G, Tsang BK (2011) P73 regulates cisplatin-induced apoptosis in ovarian cancer cells via a calcium/calpain-dependent mechanism. Oncogene 30(41):4219–4230
30. Kopp AF, Laniado M, Dammann F, Stern W, Grönewäller E, Balzer T, Schimpfky C, Claussen CD (1997) MR imaging of the liver with Resovist: safety, efficacy, and pharmacodynamic properties. Radiology 204(3):749–756
31. Kusumoto TYM, Baba H, Takahashi I, Kusumoto H, Ohno S, Sugimachi K (1993) Sequence dependence of the hyperthermic potentiation of carboplatin-induced cytotoxicity and intracellular platinum accumulation in HeLa cells. Br J Cancer 68(2):259–263
32. Ito A, Honda H, Kobayashi T (2006) Cancer immunotherapy based on intracellular hyperthermia using magnetite nanoparticles: a novel concept of "heat-controlled necrosis" with heat shock protein expression. Cancer Immunol Immunother 55(3): 320–328
33. Mitsudo K, Koizumi T, Iida M, Iwai T, Oguri S, Yamamoto N, Itoh Y, Kioi M, Hirota M, Tohnai I (2012) Thermochemoradiation therapy using superselective intra-arterial infusion via superficial temporal and occipital arteries for oral cancer with N3 cervical lymph node metastases. Int J Radiat Oncol Biol Phys 83(5):639–645
34. Fukumura H, Sato M, Kezuka K, Sato I, Feng X, Okumura S, Fujita T, Yokoyama U, Eguchi H, Ishikawa Y et al (2012) Effect of ascorbic acid on reactive oxygen species production in chemotherapy and hyperthermia in prostate cancer cells. J Physiol Sci 62(3):251–257
35. Florea A-M, Büsselberg D (2011) Cisplatin as an anti-tumor drug: cellular mechanisms of activity, drug resistance and induced side effects. Cancers 3(1):1351–1371
36. Kim H-J, Lee J-H, Kim S-J, Oh GS, Moon H-D, Kwon K-B, Park C, Park BH, Lee H-K, Chung S-Y et al (2010) Roles of NADPH oxidases in cisplatin-induced reactive oxygen species generation and ototoxicity. J Neurosci 30(11):3933–3946
37. Jäckel M, Köpf-Maier P (1991) Influence of cisplatin on cell-cycle progression in xenografted human head and neck carcinomas. Cancer Chemother Pharmacol 27(6):464–471
38. Pucci B, Kasten M, Giordano A (2000) Cell cycle and apoptosis. Neoplasia 2(4):291–299
39. Aeq B (2004) Links between apoptosis, proliferation and the cell cycle. Br J Biomed Sci 61(2):99–102

Life Sciences 101 (2014) 43–48

Contents lists available at ScienceDirect

Life Sciences

journal homepage: www.elsevier.com/locate/lifescie

Geranylgeranylacetone protects the heart via caveolae and caveolin-3

Yasuo M. Tsutsumi [a,*], Rie Tsutsumi [b], Yousuke T. Horikawa [a], Yoko Sakai [a], Eisuke Hamaguchi [a], Yoshihiro Ishikawa [c], Utako Yokoyama [c], Asuka Kasai [a], Noriko Kambe [a], Katsuya Tanaka [a]

[a] Department of Anesthesiology, University of Tokushima, Tokushima, Japan
[b] Department of Nutrition, University of Tokushima, Tokushima, Japan
[c] Cardiovascular Research Institute, Yokohama City University, Yokohama, Japan

ARTICLE INFO

Article history:
Received 5 November 2013
Accepted 12 February 2014
Available online 26 February 2014

Keywords:
Geranylgeranylacetone
Caveolin
Caveolae
Cardiac protection
Heat shock protein

ABSTRACT

Aims: Geranylgeranylacetone (GGA) is commonly utilized to protect the gastric mucosa in peptic ulcer disease. Recently GGA has been shown to protect the myocardium from ischemia/reperfusion by activating heat shock proteins. However, the exact mechanism as to how GGA activates these protective proteins is unknown. Caveolae and caveolin-3 (Cav-3) have been implicated in ischemia, anesthetic, and opioid induced cardiac protection. Given the lipophilic nature of GGA it is our hypothesis that GGA induced cardiac protection requires caveolae and Cav-3.

Main methods: We used an in vivo mouse model of ischemia–reperfusion injury and performed biochemical assays in excised hearts.

Key findings: GGA treated control mice revealed increased caveolae formation and caveolin-3 in buoyant fractions, mediating heat shock protein 70 activation. Furthermore, control mice treated with GGA were protected against ischemia/reperfusion injury whereas Cav-3 knockout (Cav-3 KO) mice were not. Troponin levels confirmed myocardial damage. Finally, Cav-3 KO mice treated with GGA were not protected against mitochondrial swelling whereas control mice had significant protection.

Significance: This study showed that caveolae and caveolin-3 are essential in facilitating GGA induced cardiac protection by optimizing spatial and temporal signaling to the mitochondria.

Introduction

Geranylgeranylacetone (GGA), an acyclic polyisoprenoid, is commonly used as an oral anti-ulcer medication in Asia. This compound has been shown to be effective in protecting the gastric mucosa against insults without affecting gastric acid secretion (Fujimoto et al., 1982; Murakami et al., 1981). Oral GGA has been demonstrated to have protective effects on myocardial ischemia/reperfusion injury within the rat heart (Ooie et al., 2001). Yamanaka et al. suggested that GGA-induced cardiac preconditioning exerted protective effects on myocardial ischemia/reperfusion injury by mediating the activation of protein kinase C and heat shock protein (HSP) (Yamanaka et al., 2003). Further investigations demonstrated that GGA also prevented cellular endothelial damage (Zhu et al., 2005), diminished apoptosis and preserved mitochondrial respiratory function (Shinohara et al., 2007).

Structural scaffolding domains commonly organize signal transduction molecules and receptors. Caveolae are small membrane invaginations of the plasma membrane that are enriched in sphingolipids, cholesterol, and lipid rafts (Lisanti et al., 1994; Palade, 1953; Patel et al., 2008). Caveolins are the structural proteins of caveolae and are present in three isoforms, caveolin (Cav)-1, -2, and -3 (Lisanti et al., 1994; Patel et al., 2008). Additionally, many signaling molecules are known to localize in caveolae and interact with the scaffolding domain of caveolin. We have recently shown that both caveolae and Cav-3 were essential for ischemic (Horikawa et al., 2008; Tsutsumi et al., 2008), anesthetic (Horikawa et al., 2008), and opioid (Tsutsumi et al., 2010b) induced cardiac protection. It is our hypothesis that caveolin-3 and caveolae are also essential in GGA induced cardiac protection.

Materials and methods

Animals

All animals were treated in compliance with the Guidelines for Proper Conduct of Animal Experiment and Related Activities (Ministry of Education, Culture, Sports, Science and Technology of Japan) and the Guideline for Care and Use of Lab Animals at the University of

* Corresponding author at: Department of Anesthesiology, University of Tokushima, 3-18-15 Kuramoto, Tokushima 770-8503, Japan. Tel.: +81 88 633 7181; fax: +81 88 633 7182.
E-mail address: tsutsumi@tokushima-u.ac.jp (Y.M. Tsutsumi).

http://dx.doi.org/10.1016/j.lfs.2014.02.019
0024-3205/

Tokushima. Animal use protocols were approved by the Animal Care and Use Committee, the University of Tokushima. Male C57BL/6 mice (8–10 weeks old, 21–26 g body weight) were purchased from Japan SLC and Cav-3 knockout (Cav-3 KO) mice were created as reported previously (Hagiwara et al., 2000). Animals were randomly assigned into treatment groups by an independent observer. The animals were kept on a 12 hour light–dark cycle in a temperature-controlled room. GGA was provided by Eisai Co., Tokyo, Japan and was given by gavage at a dose of 200 mg/kg (dissolved with 0.4% lecithin in deionized water). Mice in the control group were given the same dose of vehicle.

Electron microscopy

Wild-type mice were given GGA or vehicle by oral gavage. Twenty four hours later, whole hearts were fixed with 2.5% glutaraldehyde in 0.1 M cacodylate buffer for 2 h at room temperature, post-fixed in 1% OsO_4 in 0.1 M cacodylate buffer (1 h), and uranyl acetate, dehydrated in a graded series of ethanol solutions, and embedded in epon epoxy resin. Sections were cut with a Reichert Ultracut E Ultramicrotome (Leica Microsystems, Wetzlar, Germany) and observed with an electron microscope (Hitachi H7650, Hitachi Co., Tokyo, Japan). Random sections were taken by an electron microscopy technician blinded to the treatments.

Sucrose density membrane fractionation

We performed whole left ventricle sucrose density membrane fractions as reported previously (Tsutsumi et al., 2008). Fraction samples 4–12 were used in immunoblot analyses. We defined fractions 4–6 as lipid rich–buoyant membrane fractions enriched in caveolae and proteins associated with caveolae. Fractions 9–12 were defined as non-buoyant fractions.

Immunoblot analysis

Proteins in whole left ventricle or membrane fractions were separated by SDS-PAGE 10% polyacrylamide precast gels (Bio-Rad Laboratories) and transferred to a polyvinylidene difluoride membrane by electroelution. Membranes were blocked in PBS containing 2.0% nonfat dry milk and incubated with primary antibody overnight at 4 °C. Bound primary antibodies were visualized using secondary antibodies conjugated with horseradish peroxidase from Santa Cruz Biotechnology (Santa Cruz) and ECL reagent from Amersham Pharmacia. All displayed bands migrated at the appropriate size, as determined by comparison to molecular weight standards (Santa Cruz Biotechnology).

Immunoprecipitation

Immunoprecipitation was performed using Protein A Sepharose CL-4B (GE Healthcare) as described previously (Hirose et al., 2011). Buoyant fraction samples were incubated with primary antibody for 3 h at 4 °C, immunoprecipitated overnight with protein-agarose at 4 °C, and then centrifuged for 5 min at 13,000 g. Protein-agarose pellets were washed 3 times. Wash buffer was removed and sample buffer was added, and then boiled for 5 min at 95 °C for immunoblotting.

Ischemia–reperfusion protocol and experimental groups

Cav-3 KO and control mice were randomly assigned to receive GGA or vehicle 24 h before ischemic injury. Mice were anesthetized with pentobarbital sodium (80 mg/kg i.p.) and mechanically ventilated by using a pressure-controlled ventilator (TOPO Ventilator, Kent Scientific) as described before (Tsutsumi et al., 2006, 2007). Core temperature was maintained with a heating pad and ECG leads were placed to record heart rate. The hemodynamic effects were measured through the right carotid artery cannulation with a 1.4F Mikro-tip pressure transducer (Model SPR-671, Millar Instruments), which was connected to an amplifier (Model TC-510, Millar Instruments) for determination of heart rate, arterial blood pressure, and rate pressure product.

Lethal ischemia was produced by occluding the left coronary artery with a 7–0 silk suture placed with a tapered BV-1 needle (Ethicon) for 30 min. After 30 min of occlusion, the ligature was released and the heart was reperfused for 2 h. After reperfusion, mice were heparinized, and the coronary artery was again occluded. The area at risk (AAR) was determined by staining with 1% Evans blue (1.0 mL, Sigma). The heart was immediately excised and cut into 1.0-mm slices (McIlwain tissue chopper; Brinkmann Instruments). Each slice of left ventricle (LV) was then counterstained with 2,3,5,-triphenyltetrazolium chloride (Sigma). After overnight storage in 10% formaldehyde, slices were weighed and visualized under a microscope (SZ61-TR, Olympus) equipped with a charge coupled device camera (DXM 1200F, Nikon). The images were analyzed (Image-Pro Plus, Media Cybernetics), and area at risk (AAR) and infarct size (IS) were determined by planimetry as previously described (Tsutsumi et al., 2008; Horikawa et al., 2008). Cardiac troponin I (cTnI) levels in the serum were measured using a High Sensitivity Mouse Cardiac Troponin-I ELISA Kit (Life Diagnostics) as described before (Tsutsumi et al., 2010a).

Mitochondrial isolation and swelling assay

Mice were anesthetized and hearts were harvested, immediately rinsed with PBS, and placed in homogenizer containing 4 mL sucrose buffer A (300 mM sucrose, 10 mM Tris–HCl, 2 mM EGTA and 5 mg/mL BSA, pH 7.4) on ice. Hearts were homogenized using 10 strokes and homogenate centrifuged at 2000 ×*g* for 2 min at 4 °C to remove cell debris. The supernatant was further centrifuged at 10,000 ×*g* for 30 min at 4 °C to sediment impure mitochondria. Mitochondrial pellet was purified and washed as described previously (Fridolfsson et al., 2012). 200 μL of mitochondria in sucrose buffer B (300 mM sucrose, 10 mM Tris–HCl, pH 7.4) was loaded on to 96-well plate and challenged with 100 μM $CaCl_2$ (2 mg/mL protein concentration). Absorbance was measured every 2 s for 600 measurements at 520 nm using a VarioSkan Flash spectrophotometer (Thermo Scientific). 250 nM cyclosporine A (Sigma) pretreatment of mitochondria was used to inhibit $CaCl_2$ induced mitochondrial swelling to confirm the mitochondrial permeability transition pore (mPTP) dependence of calcium-induced swelling.

Statistical analysis

Determination of all data was performed blinded to experimental groups for the observers. Data were analyzed using Prism 6.0 (GraphPad Software, Inc.). Statistical analyses for Western blot studies were performed using Student's *t*-tests. When one-way ANOVA was needed, the Bonferroni post-hoc test was used. All data are expressed as mean ± SD. Statistical significance was defined as $P < 0.05$

Results

The effect of GGA on cardiac membrane caveolae was assessed by pre-treating mice with and without GGA and performing electron microscopy analysis. Representative electron microscopy images show that pretreatment of GGA increased membrane caveolae compared to vehicle treated control animals (Fig. 1). However, Cav-3 KO mice had significantly decreased caveolae with no significant change after GGA treatment (data not shown). To verify these findings, hearts from GGA and vehicle control animals were fractionated on a discontinuous sucrose gradient and analyzed for protein content. GGA increased both Cav-3 protein expression and HSP 70 expression in buoyant fractions 4–6, which are associated with caveolae (Fig. 2A and 2B). Additionally, immunoprecipitation experiments showed that GGA treated mice resulted in HSP 70 associated with Cav-3 in buoyant fractions (Fig. 2C), suggesting that Cav-3 is essential for HSP 70 localization and activation.

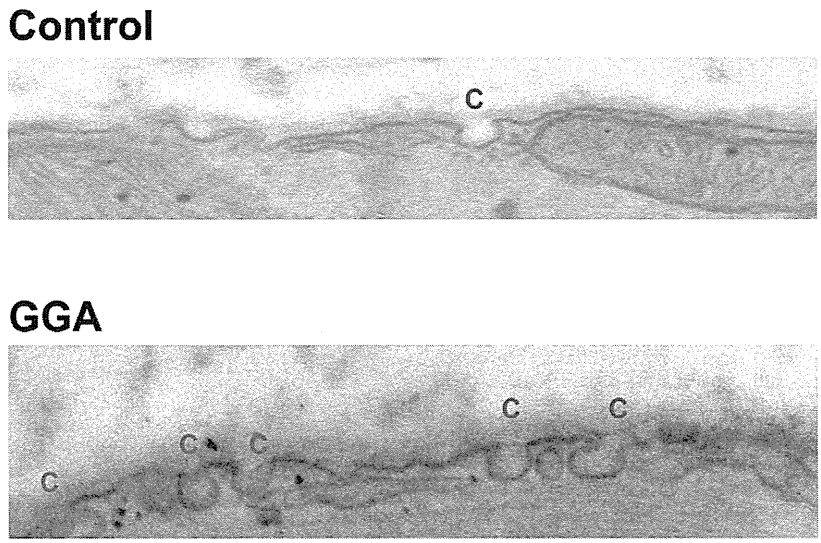

Fig. 1. Geranylgeranylacetone (GGA) increases myocardial caveolae. Electron microscopy of control and GGA treated mouse myocardium revealed a significant increase in caveolae (red C) at the sarcolemmal surface in GGA treated mice.

We found no significant differences between wild-type and Cav-3 KO mice in heart rate, blood pressure, or rate pressure product with and without GGA administration at the baseline period (Table 1). The area at risk was calculated as a percentage of the left ventricle mass and was similar between groups (Fig. 3A). Twenty-four hours after GGA administration, a significant reduction in myocardial ischemia/reperfusion injury was observed compared with vehicle control in the wild-type mice (29.0 ± 3.7% [n = 8] vs. 44.1 ± 9.3% [n = 10],

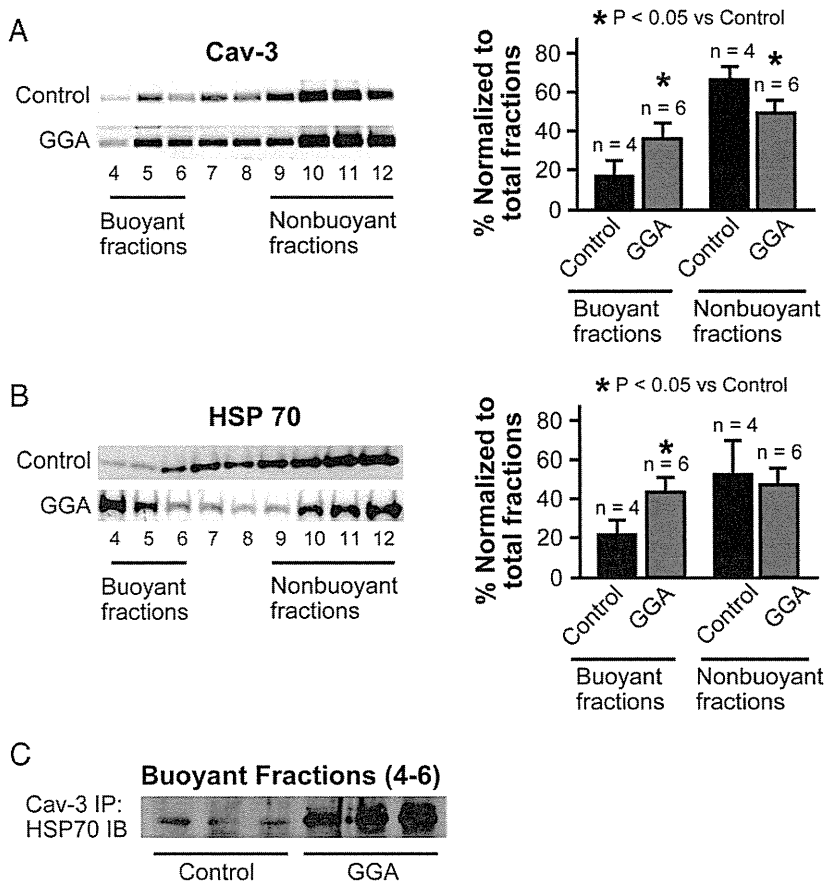

Fig. 2. Lysed and fractionated hearts on a sucrose density gradient. Fractions 4–6 were considered buoyant and 9–12 non-buoyant fractions. *P < 0.05 treated group versus control. A) and B) Fractions were collected and probed for both caveolin-3 (Cav-3) and heat shock protein 70 (HSP 70). Significant buoyant fraction localization of Cav-3 and HSP 70 was observed in geranylgeranylacetone (GGA) treated groups. C) The resulting lysates were immunoprecipitated (IP) with Cav-3 antibody and immunoblotted (IB) for HSP 70; n = 3 animals per group. There was an increased association of Cav-3 with HSP 70 after GGA administration.

Table 1
Hemodynamics parameters at baseline period.

	Control	GGA	Cav-3 KO	GGA + Cav-3 KO
Heart rate (/min)	421 ± 33	437 ± 21	413 ± 35	426 ± 37
MAP (mm Hg)	73 ± 6	69 ± 8	71 ± 4	70 ± 3
RPP (beats·min^{-1}·mm Hg·10^3)	30.5 ± 3.7	30.0 ± 3.3	29.4 ± 4.0	29.8 ± 2.3

MAP, mean arterial pressure; RPP, rate-pressure product. Data are expressed as mean ± SD.

respectively). However, in Cav-3 KO mice, this cardiac-protective effect of GGA was abolished (42.1 ± 5.2% [n = 8], Fig. 3B). Additionally, we confirmed these effects by measuring serum troponin I level, a marker of cardiac myocyte damage (Fig. 3C).

GGA reduces Ca^{2+}-induced swelling in isolated mouse heart mitochondria (Fig. 4). In wild-type mice, the addition of 100 μM Ca^{2+} caused a significant decrease in absorbance, indicating mitochondrial swelling. Ca^{2+} induced swelling was inhibited by cyclosporine A, a mPTP inhibitor, as reported previously (Tsutsumi et al., 2011). Under these conditions, GGA significantly attenuated Ca^{2+} induced swelling compared with the control; however, these effects were abolished in Cav-3 KO mice.

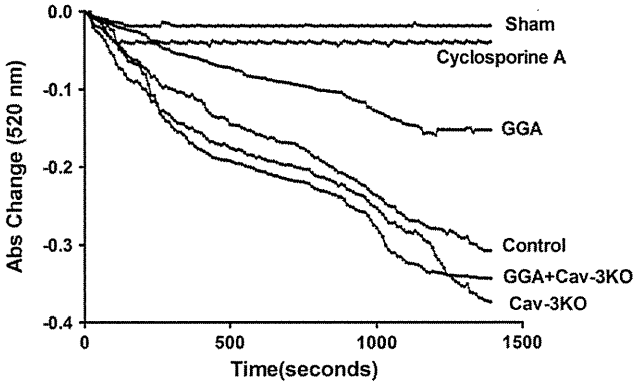

Fig. 4. Geranylgeranylacetone (GGA) inhibits mitochondrial swelling caused by ischemia-reperfusion injury. GGA treated mitochondria were isolated and revealed substantially less mitochondrial swelling compared to non-treated and Cav-3 KO mice with and without GGA when exposed to calcium chloride. Cyclosporine A was used as a control to inhibit $CaCl_2$ induced mitochondrial swelling to confirm the mitochondrial permeability transition pore (mPTP) dependence of calcium-induced swelling (n = 3).

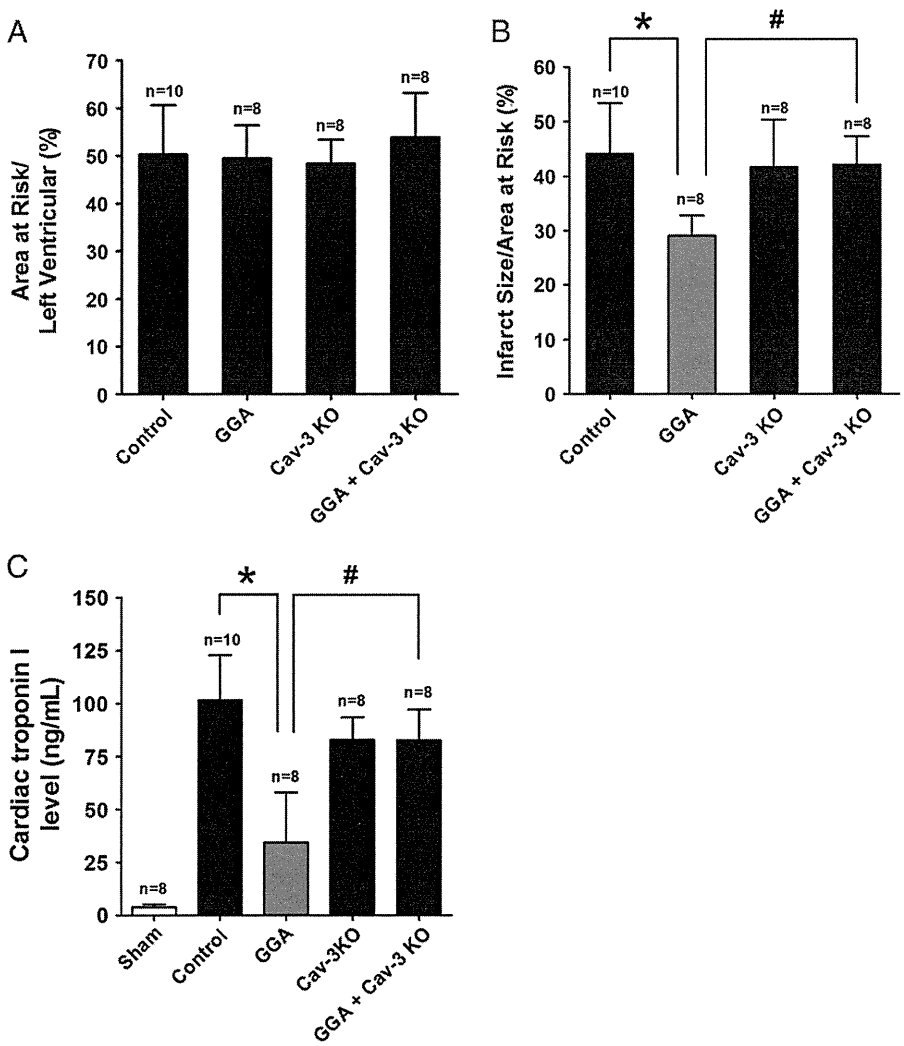

Fig. 3. Geranylgeranylacetone (GGA) protects the mouse myocardium from ischemic injury. A) Area at risk was calculated as a percentage of the left ventricle and revealed no significant differences between all groups. B) GGA was able to induce significant protection in control animals, although no protection was observed in Cav-3 KO mice. C) Cardiac troponin I, a marker of myocardial damage also revealed a significant decrease in GGA treated control mice, but no effect in Cav-3 KO mice. * $P < 0.05$; # $P < 0.05$.